Table

Sequences of Quantitative RT-PCR primers

Probe	Primer 1	Primer 2
MCP-1	5'-actgaagccagctctctcttcctc-3'	5'-ttccttcttggggtcagcacagac-3'
IL-6	5'-caatgctctcctaacagataag-3'	5'-aggcataacgcactaggt-3'
IL-1β	5'-caagcaatacccaaagaaga-3'	5'-gaaacagtccagccccatac-3'
CRP	5'-cagcttctctcggacttttg-3'	5'-aggtgttcagtggcttctttg-3'
TNFα	5'-aggtcaatctgcccaagt-3'	5'-gggctgggtagagaatg-3'
catalase	5'-aggtgttgaacgaggagga-3'	5'-ctcagcgttgtacttgtcca-3'
GST	5'-tgccaagatcaaggaacaaa-3'	5'-ccacatggtagaggagttcaa-3'
MnSOD	5'-ggtcgcttacagattgct-3'	5'-ctcccagttgattacattcc-3'
GAPDH	5'- accacagtccatgccatcac -3'	5'- tccaccaccctgttgctgta -3'

Biochemical and Biophysical Research Communications 369 (2008) 1204–1208

Contents lists available at ScienceDirect

Biochemical and Biophysical Research Communications

journal homepage: www.elsevier.com/locate/ybbrc

Identification of Glypican3 as a novel GLUT4-binding protein

Akihiko Taguchi [a], Masahiro Emoto [a], Shigeru Okuya [a,*], Naofumi Fukuda [a], Yoshitaka Nakamori [a], Mutsuko Miyazaki [a], Sachiko Miyamoto [a], Katsuya Tanabe [a], Hiroyuki Aburatani [b], Yoshitomo Oka [c], Yukio Tanizawa [a]

[a] Division of Endocrinology, Metabolism, Hematological Sciences and Therapeutics, Department of Bio-Signal Analysis, Yamaguchi University Graduate School of Medicine, 1-1-1 Minami-Kogushi, Ube, Yamaguchi, Japan
[b] Genome Science Division, Research Center for Advanced Science and Technology, University of Tokyo, Tokyo, Japan
[c] Division of Molecular Metabolism and Diabetes, Tohoku University Graduate School of Medicine, Sendai 980-8575, Japan

ARTICLE INFO

Article history:
Received 5 March 2008
Available online 14 March 2008

Keywords:
GLUT4
3T3-L1 Adipocytes
GPC3

ABSTRACT

Insulin stimulates glucose uptake in fat and muscle primarily by stimulating the translocation of vesicles containing facilitative glucose transporters, GLUT4, from intracellular compartments to the plasma membrane. Although cell surface externalization of GLUT4 is critical for glucose transport, the mechanism regulating cell surface GLUT4 remains unknown. Using a yeast two-hybrid screening system, we have screened GLUT4-binding proteins, and identified a novel glycosyl phosphatidyl inositol (GPI)-linked proteoglycan, Glypican3 (GPC3). We confirmed their interaction using immunoprecipitation and a GST pull-down assay. We also revealed that GPC3 and GLUT4 to co-localized at the plasma membrane, using immunofluorescent microscopy. Furthermore, we observed that glucose uptake in GPC3-overexpressing adipocytes was increased by 30% as compared to control cells. These findings suggest that GPC3 may play roles in glucose transport through GLUT4.

Insulin stimulation of glucose uptake into skeletal muscle and adipose tissue is achieved via the translocation of intracellular-sequestered GLUT4 protein to the cell surface membrane [1,2]. On the plasma membrane, GLUT4 proteins, responding to insulin stimulation, remain externalized for a certain period of time and facilitate glucose transport. Although cell surface externalization of GLUT4 is critical for glucose transport, the mechanism regulating cell surface GLUT4 remains largely unknown. We speculated that it would require a protein capable of interacting with the glucose transporter.

Over the past decade, several GLUT4-binding proteins, such as mUbc9 [3], TUG [4], DAXX [5], L-3-hydroxyacyl-CoA dehydrogenase [6], and carboxyl esterase [7], have been identified using the C-terminus region of GLUT4 as bait in either a two-hybrid system or an immobilized GST fusion protein pull-down experiment. For example, mUbc9 was demonstrated to regulate transporter degradation [3], whereas TUG was shown to modulate GLUT4 distribution [4]. However, the functions of other GLUT4-binding proteins are not fully understood. We speculated that a change in the three-dimensional structure of the GLUT4 partial sequence has made it difficult to identify and analyze functional GLUT4 binding proteins. Thus, we used full-length GLUT4 for screening, and thereby identified GPC3 as a GLUT4-binding protein.

GPC3 is one of the heparan sulfate proteoglycans that are anchored to the cell membrane by a glycosyl-phosphatidylinositol protein [8]. This family of proteins was shown to be related to morphogenesis and GPC3 was originally reported to be a negative regulator of cell proliferation as well as the progression of malignant tumors [9–13]. Herein, we report GPC3 as a newly identified GLUT4-binding protein. This is the first report describing a protein that acts directly on GLUT4 molecules at the plasma membrane.

Materials and methods

Antibodies. Mouse monoclonal GPC3 antibody was provided by Dr. Hiroyuki Aburatani (University of Tokyo, Japan). The following antibodies were used: anti-GLUT4 rabbit and goat, anti-GST (Santa Cruz Biotechnology, CA); anti-FLAG (M2) (Sigma); anti-Myc (9E10) (Convance, CA) and fluorescent-conjugated and horseradish peroxidase-conjugated secondary antibodies (Jackson Immuno-Research Laboratories).

Constructs. Mouse GPC3 cDNA was purchased from Open Biosystems (Huntsville, AL). Wild-type GPC3 was subcloned into a pGEX-6P1 (GE Healthcare Biosciences) vector. FLAG-tagged GPC3 and 4×Myc-tagged GLUT4-eGFP was subcloned into a pcDNA3 (Invitrogen) vector. All chemically synthesized and PCR-derived DNA sequences were verified by DNA sequencing.

Preparation of recombinant adenovirus vectors. Recombinant adenovirus encoding eGFP or FLAG-tagged GPC3 was constructed using the AdEasy adenovirus vector system according to the manufacturer's instructions (Startagene). All amplified viruses were stored at −80 °C. 3T3-L1 adipocytes were infected with recombinant adenovirus vectors encoding eGFP and FLAG-tagged GPC3 at a multiplicity of infection (m.o.i.) of 50.

* Corresponding author. Fax: +81 836 22 2342.
E-mail address: okuya@yamaguchi-u.ac.jp (S. Okuya).

0006-291X/$ - see front matter © 2008 Elsevier Inc. All rights reserved.
doi:10.1016/j.bbrc.2008.03.027

Cell culture. 3T3-L1 fibroblasts were grown in DMEM with 10% fetal bovine serum (FBS) at 37 °C. The cells (3–5 days post-confluent) were differentiated into adipocytes by incubation in the same DMEM containing 0.5 mM isobutylmethylxanthine, 0.25 μM dexamethasone, and 4 μg/ml insulin for 3 days, and then grown in DMEM with 10% FBS for an additional 3–6 days. Human hepatocellular carcinoma cell line HepG2 cells were cultured in Eagle's minimum essential medium (EMEM) with 10% FBS in at 37 °C.

Primary culture of mouse hepatocytes. Mouse hepatocytes were prepared from 5-month male C57BL/6J mice as described previously [14]. Isolated cells were seeded onto coverslips and allowed to recover for 24 h.

Yeast two-hybrid screening. The MATCHMAKER LexA Two-hybrid System (Clontech) was used for identification of GLUT4-binding proteins. As bait for screening, the vector pLexA-GLUT4 expressing a fusion protein composed of full-length rat GLUT4 linked to the DNA-binding domain was constructed. A rat adipocyte cDNA library already cloned into the pB42AD vector was obtained from Origene Technologies (Rockville, MD). Approximately 300 colonies showed activation of the yeast reporter gene, and 15 colonies showing dependence on the LexA-GLUT4 fusion protein for activation of the reporter gene were selected. Plasmids from positive clones were subsequently isolated from the yeast, transferred to E. coli, and sequenced. Full-length cDNA was obtained by 5′RACE (Rapid Amplification of cDNA End) using a kit (Clontech) and the GenBank/NCBI databases were screened for similar sequences using BLAST Search.

In vitro GST pull-down assay. GST fusion proteins of full-length GPC3 and GST alone were purified according to the manufacturer's instructions. GLUT4 protein was generated from Myc-tagged GLUT4-eGFP (four-Myc epitope-tags in the first exofacial loop and eGFP in the C-terminus) transfected 293 cells and further purified using anti-Myc antibody. These GST fusion proteins and purified 4 × Myc-tagged GLUT4-eGFP were mixed in PBS and incubated at 4 °C for 4 h. The proteins were then pulled down with glutathione-sepharose beads (GE Healthcare Biosciences).

Immunoprecipitation and immunoblotting. Cells were lysed in lysis buffer [20 mM Hepes (pH 7.2), 100 mM NaCl, 1 mM EDTA, 25 mM NaF, 1 mM sodium vanadate, 1 mM benzamidine, 5 μg/ml leupeptin, 5 μg/ml aprotinin, 1 mM PMSF, and 1 mM DTT] and the protein concentration was measured with BCA protein assay reagent (Pierce, Rockford, IL). For immunoprecipitation, the cell lysate was pre-incubated with protein-G Sepharose at 4 °C for 30 min to remove non-specific bound proteins. Then, samples were incubated with primary antibody at 4 °C for 8–12 h followed by incubation with protein-G Sepharose. Lysates and immunoprecipitates were resolved by SDS–PAGE and transferred to a polyvinylidene difluoride (PVDF) membrane (GE Healthcare Biosciences). The membranes were incubated with appropriate antibodies.

Immunofluorescence microscopy. 3T3-L1 adipocytes, HepG2 cells, and primary hepatocytes were seeded onto coverslips and allowed to recover for 24–48 h. 3T3-L1 adipocytes were serum-starved for 4 h in DMEM, followed by incubation with or without 100 nM of insulin for 15 min at 37 °C. Then, all of the cells were fixed with 3.7% formaldehyde in PBS and permeabilized with buffer A (0.5% Triton X-100 and 1% FBS in PBS) for 15 min, and finally incubated for 2 h with primary antibodies at room temperature. The cells were washed and incubated with an appropriate secondary antibody, or rhodamine-conjugated wheat germ agglutinin (Molecular Probes, Inc.) as a counter staining of cell membrane and Golgi system. The coverslips were washed thoroughly and mounted on glass slides. Immunostained cells were observed at room temperature with a laser-scanning confocal microscope (LSM5 PASCAL; Carl Zeiss Inc.).

Plasma membrane sheet assay. Cell surface protein was assayed using plasma membrane lawns as described previously [15]. The cells were subsequently swollen using hypotonic buffer and sonicated to generate a lawn of plasma membrane fragments. The membranes were immunostained with anti-GPC3 and anti-GLUT4 antibody. These cells were observed by laser confocal microscopy.

2-Deoxy-glucose uptake. Differentiated adipocytes were prepared in 24-well plates. Cells were infected with the recombinant adenoviruses. Two days thereafter, the cells were serum-starved for 2 h at 37 °C in Krebs–Ringer phosphate buffer (130 mM NaCl, 5 mM KCl, 1.3 mM $CaCl_2$, 1.3 mM $MgSO_4$, and 10 mM Na_2HPO_4, pH 7.4). The cells were then stimulated with or without 100 nM of insulin for 15 min, and deoxy-glucose uptake was determined by 2-deoxy-D-[2,6-^{3}H] glucose incorporation.

Results and discussion

Identification of GLUT4-binding proteins

Regulation of glucose uptake in muscle and adipose tissues by insulin is important for proper maintenance of blood glucose. This hormone stimulates translocation of the GLUT4 glucose transporter from the intracellular membrane to the cell surface. After translocation to the plasma membrane, GLUT4 remains on the cell surface temporarily and facilitates glucose transport. However, the mechanism regulating cell surface GLUT4 is still largely unknown. We hypothesized that it requires protein–protein interactions at the plasma membrane. We used the yeast two-hybrid screening system to identify proteins that interact physically with full-length GLUT4. As bait, we used full-length rat GLUT4 cDNA and, as prey, a rat adipose tissue cDNA library. After the first screening, we obtained more than 300 colonies. After a second screening, 15 colonies remained positive. Ultimately, nine colonies were left. Full-length cDNAs were obtained by 5′RACE. One of them was 100% identical to GPC3 [16], which was originally cloned as OCI-5, a GPI anchored membrane protein [17]. Since we also obtained mUbc9 [3], which was previously identified using the same method, our experimental procedure was thought to have worked correctly. The GPC3 sequence obtained with the yeast two-hybrid system was comprised of the residues from 521 to 597. In order to confirm the interaction between GLUT4 and GPC3, we employed the yeast two-hybrid system again; using full-length GLUT4 cDNA and full-length GPC3 cDNA as the bait and prey, respectively. We confirmed the LacZ signal indicating a direct interaction between GPC3 and GLUT4 (Fig. 1A). Next, we determined GPC3 protein expression using Western blot analysis. As shown in Fig. 1B, we detected high molecular weight form corresponding to the glycosylated GPC3 and bands corresponding to the non-glycosylated GPC3 core protein and its cleavage product of in 3T3-L1 adipocytes as in HepG2 cells. These data were consistent with the previous reports [11,13].

Intracellular localization of GPC3

The intracellular localization of GPC3 was observed in adipocytes by laser confocal microscopy. First, we determined GPC3 protein by immunofluorescent microscopy using our specific antibody against GPC3 in HepG2 cells and primary hepatocytes as a positive or negative control, respectively (Fig. 2A). As shown in Fig. 2B, most of the GPC3 was at the plasma membrane, as reported for other cell lines [17]. As expected, we observed co-localization of GLUT4 and GPC3 after insulin stimulation (Fig. 2B). Next, in order to confirm plasma membrane integrity, we prepared plasma membrane sheets from 3T3-L1 adipocytes, stained with anti-GPC3 and anti-GLUT4 antibodies, and then observed GPC3 expression by confocal microscopy (Fig. 2C). We observed that GLUT4 translocated to the plasma membrane in response to insulin stimulation. GPC3 localized at the plasma membrane on under both conditions, and merged more clearly with GLUT4 after insulin stimulation.

The results shown in Fig. 1A and Fig. 2 suggest that GPC3 interacted with GLUT4 at the plasma membrane.

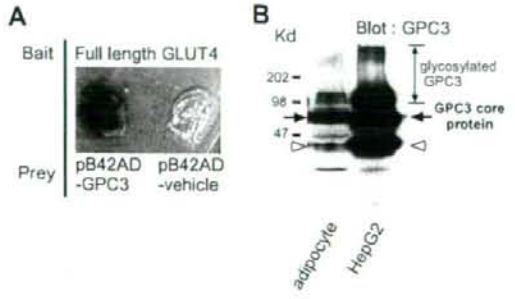

Fig. 1. Identification and expression profile of GPC3. (A) Interaction between GLUT4 and GPC3 was confirmed by the yeast two-hybrid system. Full-length cDNAs of GLUT4 and GPC3 were used as bait and prey, respectively. (B) Lysates of 3T3-L1 adipocytes and HepG2 cells were prepared, and separated by SDS–PAGE. The membrane was then blotted with anti-GPC3 antibody. HepG2 lysate was used as positive control. Arrow indicates the non-glycosylated full-length GPC3 core protein. Open arrowhead indicates a cleavage product containing the N-terminus of GPC3.

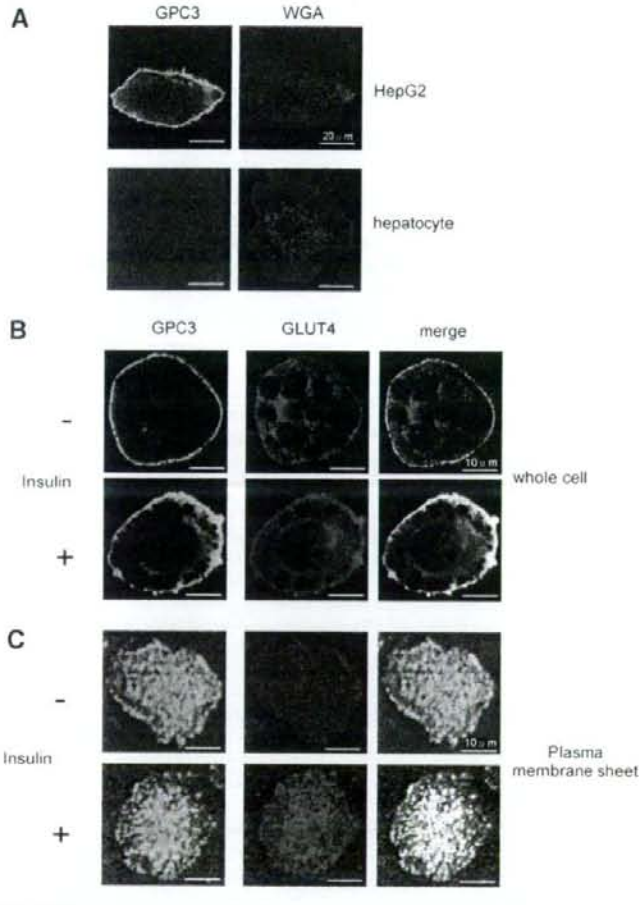

Fig. 2. Intracellular localization of GPC3. (A) Primary hepatocytes and HepG2 cells were plated on cover slips. These cells were fixed with formaldehyde and then stained using anti-GPC3 antibody followed by FITC-labeled secondary antibody. Rhodamine-conjugated wheat germ agglutinin (WGA) was used as counter staining of cell membrane and Golgi system. (B) 3T3-L1 adipocytes were serum-starved for 3–4 h and treated with or without 100 nM of insulin for 20 min. The cells were fixed with formaldehyde and stained using anti-GPC3 and anti-GLUT4 antibodies followed by appropriate FITC or Cy3 labeled secondary antibodies. These cells were observed by laser confocal microscopy. (C) 3T3-L1 adipocytes cultured on glass coverslips were treated with or without 100 nM of insulin for 15 min. At the end of each experiment, cells were rapidly washed in PBS followed by a 40 s treatment in PBS containing 0.5 mg/ml poly-L-lysine (Sigma). The cells were subsequently swollen using hypotonic buffer and sonicated to generate a lawn of plasma membrane fragments. The membranes were immunostained with anti-GPC3 and anti-GLUT4 antibody. Stained cells were observed using the confocal microscopy system as described above.

Interaction between GLUT4 and GPC3

In order to reconfirm the interaction between GPC3 and GLUT4, we conducted two other experiments; immunoprecipitation and a GST pull-down assay. First, we examined endogenous protein–protein interactions employing immunoprecipitation experiments. We prepared the total lysates of insulin-treated 3T3-L1 adipocytes. These lysates were immunoprecipitated with anti-GLUT4 antibody, and blotted with anti-GPC3 antibody. In adipocytes, we detected the interaction between GLUT4 and non-glycosylated GPC3 core protein (Fig. 3A). We also confirmed these interactions by immunoprecipitation with anti-GPC3 antibody (Fig. 3B). Second, we assessed the direct interaction between GLUT4 and GPC3 using the GST pull-down assay. We generated GST-GPC3 protein and GST alone using a bacterial system, and then purified these proteins with glutathione–sepharose beads. GLUT4 protein was purified from 293 cells transfected with 4×Myc-tagged-GLUT4-eGFP. These fusion proteins were mixed in PBS, and incubated for several hours. The proteins were then pulled down with glutathione–sepharose beads. We confirmed the GLUT4 signal in the GST-GPC3 precipitate lane, indicating a direct GLUT4 and GPC3 interaction in vitro (Fig. 3C).

Overexpression of GPC3 increased insulin stimulated glucose uptake

Since GPC3 was proved to GLUT4 at the plasma membrane, we examined whether GPC3 might regulate glucose uptake through GLUT4. We measured basal and insulin stimulated glucose uptake in 3T3-L1 adipocytes which transiently overexpressed GPC3 following transfection with adenovirus vectors. Overexpression of GPC3 increased insulin induced glucose uptake (Fig. 4). These data suggested that GPC3 overexpression to enhance insulin-stimulated glucose uptake via cell surface GLUT4.

Simpson–Golabi–Behmel syndrome (SGBS) is a rare, complex congenital syndrome with affected individuals having loss of function mutations in the GPC3 gene. Although many researchers

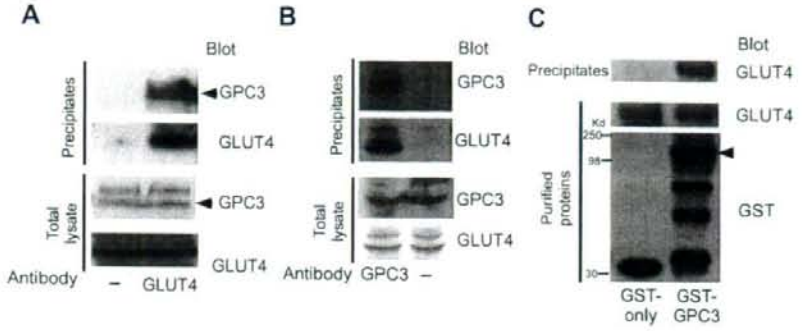

Fig. 3. GPC3 binds to GLUT4. (A) 3T3-L1 adipocytes were stimulated with 100 nM of insulin for 15 min. The lysates were incubated with or without anti-GLUT4 rabbit antibody followed by precipitation with protein A sepharose beads. Precipitates were separated by SDS–PAGE and immunoblotted with anti-GPC3 mouse monoclonal and anti-GLUT4 goat antibodies. Protein signals were visualized using horseradish peroxidase-conjugated secondary antibodies and an enhanced chemiluminescence substrate kit (GE Healthcare Biosciences). Arrowhead indicates GPC3 core protein. (B) 3T3-L1 adipocytes were stimulated with 100 nM of insulin for 15 min. Then, lysates of these adipocytes were immunoprecipitated using anti-GPC3 antibody or beads only. Precipitates were immunoblotted with anti-GLUT4 and anti-GPC3 antibodies for determination of GPC3-binding proteins. (C) GST-GPC3 and GST alone were bacterially expressed and purified by glutathione–sepharose beads. 4×Myc-tagged GLUT4-eGFP protein was expressed in 293 cells and purified using anti-Myc antibodies. Purified GST-GPC3 or GST proteins and GLUT4 protein were mixed and pulled down with glutathione–sepharose beads. The precipitates were separated by SDS–PAGE and analyzed by Western blotting using anti-GLUT4 and anti-GST antibodies. Arrowhead indicates full-length GST-GPC3.

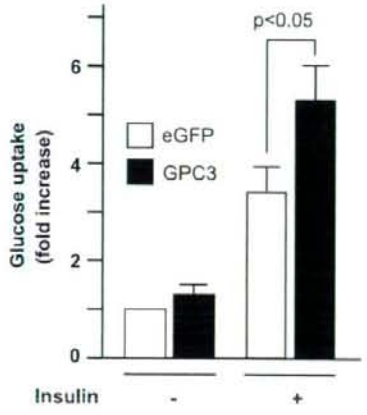

Fig. 4. Effect of GPC3 expression on glucose uptake 3T3-L1 adipocytes were infected with recombinant adenovirus vectors encoding FLAG-GPC3 or eGFP as a control at a m.o.i. of 50. The cells were serum-starved for 3 h and treated with or without 100 nM of insulin for 15 min. Glucose uptake was determined by 2-deoxy-D-[2,6^{3}H] glucose incorporation. Non-specific glucose uptake was measured in the presence of 20 μM cytochalasin B and subtracted from each determination to obtain the specific uptake. Statistical analyses were performed using Student's *t*-test. Experiments were repeated six times. Values are expressed as means ± SE, as indicated.

reported that the patients have general feature of overgrowth and cancer development, little is known about the clinical characteristics on glucose metabolism [18–21]. It was reported that some infants had hypoglycemia due to hyperplasia of islets of Langerhans rather than modification of insulin action in peripheral tissues [22]. More detailed analysis for the peripheral insulin action, especially on the adipose tissue would clarify the physiological role of GPC3 on glucose metabolism.

In conclusion, we identified a novel GLUT4-binding protein GPC3, using a yeast two-hybrid screening system. We also demonstrated GPC3 and GLUT4 to co-localized at the plasma membrane in response to insulin. Furthermore, overexpression of GPC3 increased insulin stimulated glucose uptake in cultured adipocytes. GPC3 may play a role in insulin stimulated glucose uptake.

Acknowledgments

We are also very grateful to Dr. Teruo Nishida for generously supporting us in the using a laser confocal microscope experiments. The authors thank Y. Kora and M. Kaneko for technical assistance. This study was supported in part by Grants-in-Aid for Scientific Research (17590934 to M. Emoto, 15590939 and 17590935 to S. Okuya) from the Ministry of Education, Culture, Sports, Science and Technology of Japan, and a grant from Takeda Science Foundation to S. Okuya.

References

[1] J.C. Hou, J.E. Pessin, Ins (endocytosis) and outs (exocytosis) of GLUT4 trafficking, Curr. Opin. Cell Biol. 19 (2007) 466–473.
[2] S. Huang, M.P. Czech, The GLUT4 glucose transporter, Cell Metab. 5 (2007) 237–252.
[3] F. Giorgino, O. de Robertis, L. Laviola, C. Montrone, S. Perrini, K.C. McCowen, R.J. Smith, The sentrin-conjugating enzyme mUbc9 interacts with GLUT4 and GLUT1 glucose transporters and regulates transporter levels in skeletal muscle cells, Proc. Natl. Acad. Sci. USA 97 (2000) 1125–1130.
[4] J.S. Bogan, N. Hendon, A.E. McKee, T.S. Tsao, H.F. Lodish, Functional cloning of TUG as a regulator of GLUT4 glucose transporter trafficking, Nature 425 (2003) 727–733.
[5] V.S. Lalioti, S. Vergarajauregui, D. Pulido, I.V. Sandoval, The insulin-sensitive glucose transporter, GLUT4, interacts physically with Daxx. Two proteins with capacity to bind Ubc9 and conjugated to SUMO1, J. Biol. Chem. 277 (2002) 19783–19791.
[6] Y. Shi, S.J. Samuel, W. Lee, C. Yu, W. Zhang, M. Lachaal, C.Y. Jung, Cloning of an L-3-hydroxyacyl-CoA dehydrogenase that interacts with the GLUT4 C-terminus, Arch. Biochem. Biophys. 363 (1999) 323–332.
[7] W. Lee, J. Ryu, J. Hah, T. Tsujita, C.Y. Jung, Association of carboxyl esterase with facilitative glucose transporter isoform 4 (GLUT4) intracellular compartments in rat adipocytes and its possible role in insulin-induced GLUT4 recruitment, J. Biol. Chem. 275 (2000) 10041–10046.
[8] J. Filmus, Glypicans in growth control and cancer, Glycobiology 11 (2001) 19R–23R.
[9] D.F. Cano-Gauci, H.H. Song, H. Yang, C. McKerlie, B. Choo, W. Shi, R. Pullano, T.D. Piscione, S. Grisaru, S. Soon, L. Sedlackova, A.K. Tanswell, T.W. Mak, H. Yeger, G.A. Lockwood, N.D. Rosenblum, J. Filmus, Glypican-3-deficient mice exhibit developmental overgrowth and some of the abnormalities typical of Simpson–Golabi–Behmel syndrome, J. Cell Biol. 146 (1999) 255–264.
[10] H. Lin, R. Huber, D. Schlessinger, P.J. Morin, Frequent silencing of the GPC3 gene in ovarian cancer cell lines, Cancer Res. 59 (1999) 807–810.
[11] Y. Midorikawa, S. Ishikawa, H. Iwanari, T. Imamura, H. Sakamoto, K. Miyazono, T. Kodama, M. Makuuchi, H. Aburatani, Glypican-3, overexpressed in hepatocellular carcinoma, modulates FGF2 and BMP-7 signaling, Int. J. Cancer 103 (2003) 455–465.
[12] H.H. Song, W. Shi, Y.Y. Xiang, J. Filmus, The loss of glypican-3 induces alterations in Wnt signaling, J. Biol. Chem. 280 (2005) 2116–2125.

[13] M.I. Capurro, W. Shi, S. Sandal, J. Filmus, Processing by convertases is not required for glypican-3-induced stimulation of hepatocellular carcinoma growth, J. Biol. Chem. 280 (2005) 41201–41206.
[14] J.D. Horton, H. Shimano, R.L. Hamilton, M.S. Brown, J.L. Goldstein, Disruption of LDL receptor gene in transgenic SREBP-1a mice unmasks hyperlipidemia resulting from production of lipid-rich VLDL, J. Clin. Invest. 103 (1999) 1067–1076.
[15] M. Emoto, S.E. Langille, M.P. Czech, A role for kinesin in insulin-stimulated GLUT4 glucose transporter translocation in 3T3-L1 adipocytes, J. Biol. Chem. 276 (2001) 10677–10682.
[16] J. Filmus, J.G. Church, R.N. Buick, Isolation of a cDNA corresponding to a developmentally regulated transcript in rat intestine, Mol. Cell. Biol. 8 (1988) 4243–4249.
[17] K. Watanabe, H. Yamada, Y. Yamaguchi, K-Glypican: a novel GPI-anchored heparan sulfate proteoglycan that is highly expressed in developing brain and kidney, J. Cell Biol. 130 (1995) 1207–1218.
[18] G. Pilia, R.M. Hughes-Benzie, A. MacKenzie, P. Baybayan, E.Y. Chen, R. Huber, G. Neri, A. Cao, A. Forabosco, D. Schlessinger, Mutations in GPC3, a glypican gene, cause the Simpson–Golabi–Behmel overgrowth syndrome, Nat. Genet. 12 (1996) 241–247.
[19] N. Okamoto, M. Yagi, K. Imura, Y. Wada, A clinical and molecular study of a patient with Simpson–Golabi–Behmel syndrome, J. Hum. Genet. 44 (1999) 327–329.
[20] S. Lindsay, M. Ireland, O. O'Brien, J. Clayton-Smith, J.A. Hurst, J. Mann, T. Cole, J. Sampson, S. Slaney, D. Schlessinger, J. Burn, G. Pilia, Large scale deletions in the GPC3 gene may account for a minority of cases of Simpson–Golabi–Behmel syndrome, J. Med. Genet. 34 (1997) 480–483.
[21] J.Y. Xuan, A. Besner, M. Ireland, R.M. Hughes-Benzie, A.E. MacKenzie, Mapping of Simpson–Golabi–Behmel syndrome to Xq25–q27, Hum. Mol. Genet. 3 (1994) 133–137.
[22] M.R. DeBaun, J. Ess, S. Saunders, Simpson–Golabi–Behmel syndrome: progress toward understanding the molecular basis for overgrowth, malformation, and cancer predisposition, Mol. Genet. Metab. 72 (2001) 279–286.

THE JOURNAL OF COMPARATIVE NEUROLOGY 510:1–23 (2008)

Wolfram Syndrome 1 (*Wfs1*) Gene Expression in the Normal Mouse Visual System

JUNE KAWANO,[1,2]* YUKIO TANIZAWA,[3] AND KOH SHINODA[2]

[1]Laboratory for Neuroanatomy, Department of Neurology, Kagoshima University Graduate School of Medical and Dental Sciences, Kagoshima, 890-8544, Japan

[2]Division of Neuroanatomy, Department of Neuroscience, Yamaguchi University School of Medicine, Ube, Yamaguchi, 755-8505, Japan

[3]Division of Endocrinology, Metabolism, Hematological Sciences and Therapeutics,Department of Bio-Signal Analysis, Yamaguchi University Graduate School of Medicine, Ube, Yamaguchi, 755-8505, Japan

ABSTRACT

Wolfram syndrome (OMIM 222300) is a neurodegenerative disorder defined by insulin-dependent diabetes mellitus and progressive optic atrophy. This syndrome has been attributed to mutations in the *WFS1* gene, which codes for a putative multi-spanning membrane glycoprotein of the endoplasmic reticulum. The function of WFS1 (wolframin), the distribution of this protein in the mammalian visual system, and the pathogenesis of optic atrophy in Wolfram syndrome are unclear. In this study we made a detailed analysis of the distribution of *Wfs1* mRNA and protein in the normal mouse visual system by using in situ hybridization and immunohistochemistry. The mRNA and protein were observed in the retina, optic nerve, and brain. In the retina, Wfs1 expression was strong in amacrine and Müller cells, and moderate in photoreceptors and horizontal cells. In addition, it was detectable in bipolar and retinal ganglion cells. Interestingly, moderate Wfs1 expression was seen in the optic nerve, particularly in astrocytes, while little Wfs1 was expressed in the optic chiasm or optic tract. In the brain, moderate Wfs1 expression was observed in the zonal, superficial gray, and intermediate gray layers of the superior colliculus, in the dorsomedial part of the suprachiasmatic nucleus, and in layer II of the primary and secondary visual cortices. Thus, *Wfs1* mRNA and protein were widely distributed in the normal mouse visual system. This evidence may provide clues as to the physiological role of Wfs1 protein in the biology of vision, and help to explain the selective vulnerability of the optic nerve to WFS1 loss-of-function. J. Comp. Neurol. 510:1–23, 2008.

Indexing terms: in situ hybridization; immunohistochemistry; retina; optic nerve; optic atrophy; wolframin; glutamine synthetase

Wolfram syndrome (OMIM 222300) is an autosomal recessive neurodegenerative disorder defined by juvenile-onset nonautoimmune insulin-dependent diabetes mellitus and progressive optic atrophy (Wolfram and Wagener, 1938). The nuclear gene responsible for Wolfram syndrome was mapped to human chromosome 4 at p16.1 (Polymeropoulos et al., 1994; Collier et al., 1996), and was subsequently identified as *WFS1* (Wolfram syndrome 1) or *wolframin* (Inoue et al., 1998; Strom et al., 1998). The *WFS1* gene encodes a putative 890-amino acid protein with an apparent molecular mass of ≈100 kDa (Inoue et al., 1998; Strom et al., 1998). The subcellular localization of WFS1 protein (wolframin) has been assigned primarily to the endoplasmic reticulum (ER) membrane. WFS1 protein contains nine transmembrane segments and is embedded in the ER membrane with the amino-terminus in the cytosol and the carboxy-terminus in the ER lumen (Takeda et al., 2001; Hofmann et al., 2003). Subsequent functional studies demonstrated that WFS1 protein is im-

Grant sponsor: Japan Society for the Promotion of Science (JSPS); Grant numbers: Grant-in-Aid for Scientific Research (C) (15591228 to J.K.); Grant-in-aid for Scientific Research (C) (17500231 to K.S.); Grant sponsor: The Ministry of Education, Culture, Sports, Science and Technology (MEXT); Grant number: Grant-in-aid for Scientific Research on Priority Areas (19040020 to K.S.); Grant sponsor: Kodama Memorial Fund Medical Research; Grant number: 2006-100 (to J.K.).

*Correspondence to: June Kawano, MD, PhD, Laboratory for Neuroanatomy, Department of Neurology, Kagoshima University Graduate School of Medical and Dental Sciences, 35-1, Sakuragaoka 8-chome, Kagoshima, 890-8544, Japan. E-mail: kawanoj@m2.kufm.kagoshima-u.ac.jp

Received 6 November 2006; Revised 3 June 2008; Accepted 20 March 2008

DOI 10.1002/cne.21734

Published online in Wiley InterScience (www.interscience.wiley.com).

portant in the regulation of intracellular Ca^{2+} homeostasis and its expression is induced under conditions of troubled homeostasis, including ER stress (Osman et al., 2003; Yamaguchi et al., 2004; Ueda et al., 2005; Takei et al., 2006). In addition, mutation screening analyses in Wolfram syndrome patients showed more than 50 distinct mutations of the *WFS1* gene, including stop, frameshift, deletion, and missense mutations (Inoue et al., 1998; Strom et al., 1998; Hardy et al., 1999; Gómez-Zaera et al., 2001; Khanim et al., 2001; Tessa et al., 2001). Thus, loss-of-function mutations in the *WFS1* gene have been linked to Wolfram syndrome. However, roles of WFS1 protein in cellular functions and the mechanism by which mutations of the *WFS1* gene cause Wolfram syndrome remain unclear.

The association of diabetes mellitus and optic atrophy has been known since at least 1858 when von Gräfe reported optic atrophy as a complication of diabetes mellitus (von Gräfe, 1858). This report is probably the first description of Wolfram syndrome (Minton et al., 2003). The prevalence of Wolfram syndrome is one per 770,000 in the UK population and the median age of onset of optic atrophy is 11 years (Barrett et al., 1995). The ophthalmologic signs are a progressive decrease in visual acuity, constriction of the peripheral visual field with or without central scotoma, color vision disturbance, and bilateral optic disc atrophy. Diabetic retinopathy is a rare complication (Mtanda et al., 1986; Seynaeve et al., 1994; Barrett et al., 1997). Although a profound reduction in visual function is observed in Wolfram syndrome patients, the electroretinogram (ERG) tests indicate normal or only slightly reduced responses (Niemeyer and Marquardt, 1972; Mtanda et al., 1986; Seynaeve et al., 1994; Barrett et al., 1997). These findings suggest that the site of pathology for optic atrophy lies not in the retina, but in the visual pathway proximal (posterior) to the eye including the optic nerve (Barrett et al., 1997). In addition, brains of Wolfram syndrome patients showed neuronal loss and gliosis in the lateral geniculate nucleus (LGN) and superior colliculus (SC) as well as severe degeneration of the optic nerve (Genís et al., 1997; Shannon et al., 1999). Thus, ophthalmologic and neuropathological facts concerning optic atrophy in Wolfram syndrome have been accumulated. However, the site of pathology, i.e., causative cell types, for the optic atrophy remains unclear. To obtain insights into causative cell types for optic atrophy it is necessary to examine *WFS1* expression not only in the retina but also in the optic nerve, the optic chiasm, the optic tract, and in the retino-recipient nuclei, since there is a possibility that the optic atrophy is due to neuronal loss in the retino-recipient nuclei caused by loss-of-function mutations in the *WFS1* gene (retrograde transsynaptic degeneration). Insights into the causative cell types may provide hypotheses about the pathogenesis of optic atrophy in Wolfram syndrome.

In the rodent central nervous system (CNS), *Wfs1* expression has previously been described in neurons of the cerebral cortex, the basal ganglia, the hypothalamus, the brainstem motor and sensory nuclei, the reticular formation, and the cerebellar cortex, as well as in hippocampal CA1 pyramidal neurons (Takeda et al., 2001, Ishihara et al., 2004). In the visual system, recent studies suggest that WFS1 protein is expressed in retinal ganglion cells (RGCs) and optic nerve glia of the cynomolgus monkey (Yamamoto et al., 2006). To know species differences in the localization of WFS1 protein in the visual system, to obtain insights into causative cell types for optic atrophy in Wolfram syndrome, and to establish a basis for functional studies of WFS1 in the visual system, we performed a detailed histochemical analysis of the distribution of *Wfs1* mRNA and protein in the normal mouse visual system including the retina, the optic nerve, the optic chiasm, the optic tract, the retino-recipient nuclei, and the visual cortex.

MATERIALS AND METHODS

Animals and tissue preparation

Male mice (n = 24; 7–8 weeks old; C57BL/6NCrlCrlj; Charles River Laboratories Japan, Yokohama, Kanagawa, Japan) were used in this study. Seven-week-old mice were used for the retrograde labeling of RGCs and 8-week-old mice for immunoblot and histochemistry.

For immunoblot analysis the mice were deeply anesthetized with sodium pentobarbital (50 mg/kg, i.p.). The brain, retina, and optic nerve were dissected from the skull on ice, immediately frozen in liquid nitrogen, and stored at –70°C prior to use. For histochemistry by using frozen sections the mice were deeply anesthetized with sodium pentobarbital (50 mg/kg, i.p.) and perfused transcardially with 4% paraformaldehyde dissolved in 0.1 M sodium phosphate buffer (PB; pH 7.4) at 4°C. The eyeballs including the optic nerve and the brain were removed from the skull, stored in the same fixative for 48 hours, and then immersed in 30% saccharose in 0.1 M PB at 4°C until they sank. The eyeballs including the optic nerve were frozen in powdered dry ice and sectioned in the meridian plane at a thickness of 25 μm on a cryostat. The brains were frozen and coronally cut at a thickness of 40 μm. The sections were collected in a cryoprotectant medium (33.3% saccharose, 1% polyvinylpyrrolidone (K-30), and 33.3% ethylene glycol in 0.067 M sodium PB (pH 7.4) containing 0.067% sodium azide; Warr et al., 1981) and stored at –30°C prior to use. For immunohistochemistry by using whole-mount retinae the mice were anesthetized and perfused as described above. The eyeballs were removed from the skull and stored in the same fixative for 48 hours. The retina was gently dissected and immersed in 30% saccharose in 0.1 M PB at 4°C until they sank. The retina was shock-frozen in acetone at –70°C and stored in a freezer at the same temperature prior to use.

All experimental protocols for this study were approved by the committees on the Ethics of Animal Experimentation at Kagoshima University or at Yamaguchi University School of Medicine. The protocols were conducted according to the guidelines for Animal Research of Kagoshima University or Yamaguchi University School of Medicine and The Law (No. 105) and Notification (No. 6) of the Japanese Government.

Retrograde labeling of retinal ganglion cells

Seven-week-old mice were anesthetized with a mixture containing ketamine hydrochloride (60 mg/kg, i.p.) and xylazine (6 mg/kg, i.p.). A full-strength solution of Fluorescent Latex Microspheres (Red fluorescent RetroBeads; rhodamine label, Lumafluor, Naples, FL) was stereotaxically injected through a glass micropipette (20–30 μm in tip diameter) by air pressure. The injection was made into the bilateral SC (six mice). After a period of 4 days the mice

were reanesthetized and perfused as described above. In addition, Fluoro-Ruby (dextran-tetramethylrhodamine, Molecular Probes, Eugene, OR) was used as another retrograde tracer. A 10% (w/v) solution dissolved in saline was injected. The injection was made into the bilateral LGN (two mice), the bilateral SC (two mice), or both the bilateral LGN and the bilateral SC (two mice). The survival period was set at 3–5 days. Other procedures were the same as those in the Fluorescent Latex Microspheres injection cases.

Antibodies

Preparation of the affinity-purified rabbit anti-Wfs1 N-terminus (anti-Wfs1) antibody recognizing the N-terminus 179 amino acids of mouse Wfs1 protein was described previously (Cryns et al., 2003). In brief, a cDNA fragment encoding the N-terminal 290 amino acids of mouse Wfs1 was cloned into pGEX-6P-1 plasmid (Amersham Biosciences, Tokyo, Japan) to produce chimeric proteins consisting of the N-terminal sequence of Wfs1 (1–290) and the C-terminal glutathione *S*-transferase (GST) protein, termed GST-Wfs1N. The cDNA encoding the N-terminal 179 amino acids of mouse Wfs1 was also cloned into the pMAL-c2 plasmid (New England Biolabs, Ipswich, MA) to produce a fusion protein consisting of the N-terminal sequence of mouse Wfs1 and maltose-binding protein (MBP), termed Wfs1N-MBP. The GST-Wfs1N and Wfs1N-MBP chimeric proteins were expressed in *Escherichia coli* (JM109 strain) and induced by 1 mM isopropyl-thiogalactopyranoside (IPTG). Bacterial lysates were mixed with glutathione Sepharose 4B (Amersham Biosciences) and amylose resin (New England Biolabs) for purification of GST-Wfs1N and Wfs1N-MBP. The bound GST-Wfs1N chimeric protein was eluted from glutathione Sepharose 4B by addition of 10 mM reduced glutathione solution. The eluted GST-Wfs1N chimeric protein was used for immunizing Japanese White rabbits. Rabbit antisera were collected and affinity-purified by using Wfs1N-MBP bound to the amylose resin.

The following antibodies were obtained from commercial suppliers and applied in order to label specific cell types of the retina and optic nerve. Horizontal cells and nondisplaced amacrine cells were immunolabeled with a mouse monoclonal antibody against calbindin-D-28K (Haverkamp and Wässle, 2000). Rod and (putative) ON-cone bipolar cells were immunostained with a mouse monoclonal antibody against G-protein Goα (Haverkamp and Wässle, 2000). Cholinergic amacrine cells were labeled with a goat polyclonal antibody against choline acetyltransferase (ChAT) (Jeon et al., 1998; Haverkamp and Wässle, 2000; Kang et al., 2004). RGCs including their dendrites and axons were immunolabeled with a mouse monoclonal antibody against tubulin, βIII isoform (Sharma and Netland, 2007). According to the criteria of Sharma and Netland (2007), large cells intensely labeled with this antibody in the GCL were recognized as RGCs. Nuclei of RGCs were immunostained with a mouse monoclonal antibody against Brn-3a POU-domain transcription factor (Xiang et al., 1995). Müller cells and glial cells in the optic nerve were labeled with a mouse monoclonal antibody against glutamine synthetase (Haverkamp and Wässle, 2000). Astrocytes were immunolabeled with a rabbit serum or a mouse monoclonal antibody against glial fibrillary acidic protein (GFAP) (Morcos and Chan-Ling, 2000). As for the anti-GFAP rabbit serum, this serum stains a single protein band of 51 kDa in the mouse brain on immunoblot (Jalil et al., 2005). Oligodendrocytes were immunostained with a mouse monoclonal antibody against oligodendrocytes [RIP] (Friedman et al., 1989). Specificity of this antibody was strictly verified in the rat CNS (Friedman et al., 1989). In the rat cerebellum, strong RIP staining was mainly confined to the white matter, although moderate RIP staining was distributed in the granular layer. In the molecular layer, composed of the unmyelinated parallel fibers, RIP staining was hardly detected (Friedman et al., 1989). In the mouse cerebellum the staining pattern of this antibody (data not shown) was identical to that in the rat cerebellum. In the mouse optic nerve the staining pattern was also identical to that in the rat (Saari et al., 1997; Morcos and Chan-Ling, 2000). Microglia were labeled with a rat monoclonal antibody against mouse CD11b (Mac-1 α chain) (Dräger, 1983; Reichert and Rotshenker, 1996). The staining patterns of these antibodies were identical to those previously published and their source, host species, antigen, and specificity are listed in Table 1.

Immunoblot analysis

The tissue of the brain, retina, and optic nerve was homogenized in phosphate-buffered saline (PBS) containing 1 mM dithiothreitol (DTT) by repeated passages through a 25G needle and then centrifuged at 500*g* for 10 minutes at 4°C to remove debris. Protein concentration of the supernatant was determined by the Bio-Rad DC Protein Assay (Bio-Rad Laboratories, Hercules, CA). The supernatant was mixed with SDS-PAGE sample buffer and boiled for 5 minutes. Forty μg of protein for brain and retina samples or 20 μg of protein for optic nerve sample were loaded onto 5–20% precast polyacrylamide gradient gels (Atto, Tokyo, Japan). The proteins were electrotransferred to a polyvinylidene difluoride (PVDF) membrane in Tris-glycine-methanol transfer buffer. The membrane was blocked for 1 hour at room temperature in buffer 1 (150 mM NaCl, and 100 mM Tris-HCl, pH 7.5) containing 2% blocking reagent (Roche Diagnostics, Penzberg, Germany) (buffer 2) and then incubated for 16 hours at 4°C with the anti-Wfs1 antibody (1:1,000) in blocking solution (buffer 2). The membrane was then rinsed with PBS three times and incubated for 1 hour at room temperature with peroxidase-conjugated affinipure $F(ab')_2$ fragment goat antirabbit IgG (H+L) (1:2,000) (Jackson ImmunoResearch Laboratories, West Grove, PA). Antigen-antibody complexes were visualized by enhanced chemiluminescence (ECL) system (GE Healthcare UK, Buckinghamshire, UK) and exposed onto Fuji medical x-ray films (RX-U) (Fujifilm, Tokyo, Japan).

To determine the specificity of anti-Wfs1 antibody we preabsorbed the antibody with GST-Wfs1N chimeric protein (antigen). The antigen (50 μg/mL) was incubated with the anti-Wfs1 antibody (1:1,000) for 3 hours at 4°C before incubation with the PVDF membrane, then the immunoblot was performed as described above. The GST-Wfs1N chimeric protein was newly generated. The service offered by Hokudo (Sapporo, Japan) was used to produce the protein. The protocols were the same as described above except for the strain of *E. coli*. For expression of the protein the B21(DE3)RIL strain was used instead of the JM109 strain.

TABLE 1. Primary Antibodies Used in This Study

Antibody	Manufacturer	Catalog No.	Lot No.	Antibody isotype	Clone	Dilution	Antigen	Specificity
Mouse Wfs1	This Study			Rabbit serum		1:5000-1:10000	Amino acids 1-179 representing N-terminus Wfs1 protein of mouse origin	A single band of ~100 kDa in extracts from the mouse brain and optic nerve. ~100 kDa and ~70 kDa bands in extracts from the mouse retina. Antigen block of immunolabeling. Figs. 1 and 2D
Calbindin-D-28K	Sigma-Aldrich, St. Louis, MO	C9848	113K4867	Mouse IgG_1	Clone CB-955	1:500	Purified bovine kidney calbindin-D-28K	A single 28-kDa band.[1] Staining pattern identical to published data[2]
Goα	Chemicon, Temecula, CA	MAB3073	24040782	Mouse IgG_1	Clone 2A	1:250	Purified bovine brain Goα	A single protein band of 39-42 kDa.[1] Staining pattern identical to published data[2]
Choline Acetyltransferase	Chemicon	AB144P	24030848	Goat serum		1:100	Choline acetyltransferase from human placenta	Staining pattern identical to published data[3]
Tubulin, βIII isoform	Chemicon	MAB1637	25010305	Mouse IgG_1	Clone TU-20	1:50	A synthetic peptide corresponding to amino acids 443-450 (ESESQGPK) of human class III β-tubulin conjugated to keyhole limpet hemocyanin (KLH), a carrier for haptens	A single protein band of 50 kDa in extracts from the porcine brain[4]
Brn-3a	Santa Cruz Biotechnology, Santa Cruz, CA	sc-8429	L1106	Mouse IgG_{2b}	Clone 14A6	1:50	Amino acids 1-109 representing N-terminus Brn-3a protein of mouse origin	Staining pattern identical to published data[5]
Glutamine Synthetase	BD Biosciences Pharmingen, San Diego, CA	610517	01915	Mouse IgG_{2a}	Clone 6	1:500	Sheep glutamine synthetase (1-373: Full Length)	A single protein band of 45 kDa in extracts from the rat brain[6]
Glial Fibrillary Acidic Protein (GFAP)	Chemicon	AB5804	23080114	Rabbit serum		1:1000	Purified bovine GFAP	A single protein band of 51 kDa in extracts from the mouse brain[7]
GFAP	Chemicon	MAB360	25040157	Mouse IgG_1	Clone GA5	1:1000	Purified GFAP from porcine spinal cord	A single protein band of 51 kDa in extracts from a human glioma cell line.[8] Staining pattern (Fig. 8B) identical to that of the anti-GFAP rabbit serum (Fig. 6A)
Oligodendrocytes (RIP)	Chemicon	MAB1580	25040064	Mouse IgG_1	Clone NS-1	1:100000	Rat olfactory bulb	Staining pattern identical to published data[9]
Mouse CD11b (Mac-1 α chain)	BD Biosciences Pharmingen	550282	01651	Rat (DA) $IgG_{2b,\kappa}$	Clone M1/70	1:50	C57BL/10 mouse splenic T cells and concanavalin A-activated C57BL/10 splenocytes	Staining pattern identical to published data[10]

[1]Manufacturer's technical information; Gargini et al., 2007.
[2]Haverkamp and Wässle, 2000.
[3]Jeon et al., 1998; Haverkamp and Wässle, 2000; Kang et al., 2004.
[4]Manufacturer's technical information; Dráberová et al., 1998.
[5]Xiang et al., 1995.
[6]Manufacturer's technical information.
[7]Jalil et al., 2005.
[8]Manufacturer's technical information; Debus et al., 1983.
[9]Saari et al., 1997; Morens and Chan-Ling, 2000.
[10]Retina: Dräger, 1983; Optic nerve: Reichert and Rotshenker, 1996; Neufeld, 1999.

In situ hybridization histochemistry

To synthesize a cRNA probe for in situ hybridization an 870-base fragment of the mouse *Wfs1* cDNA was amplified by reverse-transcriptase polymerase chain reaction (RT-PCR) and subcloned into the vector pCR-Blunt (Invitrogen, Carlsbad, CA). The primers used were No. 00276, 5′-CGG GAT CCA TGA ACT CAG GCA CCC CAC CT-3′, and No. 00277, 5′-GGA ATT CCA CCT TCT GGC GTA GTG GCA G-3′. The fragment encoded the 5′-end of the protein-coding region, including all of exon 2 and the first triplet of exon 3. Two independent clones containing the insert with a different orientation (pCR-clone 3 for sense, pCR-clone 9 for antisense) were used. A sense or an antisense cRNA probe was obtained by in vitro transcription with a DIG RNA labeling kit (SP6/T7; Roche Diagnostics).

In situ hybridization histochemistry was carried out as described previously (Fujinaga et al., 2004). Free-floating sections washed for 5 minutes in diethylpyrocarbonate-treated PBS (DEPC-PBS) were pretreated with 0.2 N HCl for 20 minutes, washed twice for 5 minutes in DEPC-PBS, and then acetylated in 0.1 M triethanolamine-HCl (pH 8.0) containing 0.25% acetic anhydride for 10 minutes. Before the hybridization step, sections were washed again twice for 5 minutes with DEPC-PBS. All pretreatments were performed at 4°C. Following the pretreatment, sections were preincubated in hybridization buffer (50% deionized-formamide; 10 mM Tris-HCl, pH 7.5; 1 mM EDTA, pH 8.0; 600 mM NaCl; 1 × Denhardt's solution; 10% dextran sulfate; 0.25% sodium dodecyl sulfate; and 200 μg/mL yeast tRNA) at 55°C for 1 hour and then hybridized with DIG-labeled anti-sense cRNA probes (0.5 μg/mL; denatured at 95°C for 5 minutes and cooled at 4°C for 5 minutes shortly before use) in the same buffer at 55°C for 16 hours. After hybridization, the sections were washed with 2 × SSC (300 mM NaCl, and 30 mM sodium citrate, pH 7.0) containing 50% formamide at 55°C for 1 hour, rinsed in wash buffer (500 mM NaCl, 10 mM Tris-HCl, pH 8.0, and 1 mM EDTA, pH 8.0) for 10 minutes, and then incubated with RNase A (20 μg/mL; Sigma-Aldrich, St. Louis, MO) in wash buffer at 37°C for 30 minutes. After being rinsed in wash buffer again for 10 minutes, they were soaked in 2 × SSC containing 50% formamide and 0.2 × SSC containing 50% formamide at 55°C for 30 minutes each. To perform the immunoreaction the sections were blocked in buffer 2 (buffer 1 [150 mM NaCl, and 100 mM Tris-HCl, pH 7.5] containing 2% blocking reagent) at 20°C for 1 hour and then incubated in buffer 2 containing alkaline phosphatase-conjugated sheep anti-DIG antibody (Roche Diagnostics) diluted 1:3,000 at 20°C for 16 hours. After two washes in buffer 1 for 10 minutes they were rinsed in buffer 3 (100 mM NaCl, 50 mM $MgCl_2$, 100 mM Tris-HCl, pH 9.5) for 5 minutes and incubated with NBT/BCIP substrate (1:50; Roche Diagnostics) in buffer 3 at 37°C for 2–4 hours to visualize the immunocomplex. The coloring reaction was stopped with buffer 4 (1 mM EDTA, and 10 mM Tris-HCl, pH 8.0), and the sections were washed in PBS, mounted on glass slides using a 0.6% gelatin solution, and air-dried. The slides were coverslipped with VectaMount mounting medium (Vector Laboratories, Burlingame, CA). As a control, a sense cRNA probe was used instead of the antisense cRNA probe. Signals detected by the antisense *Wfs1* cRNA probe were categorized as positive if they were stronger than those detected by the sense probe in an adjacent section (control section).

Immunohistochemistry

Single immunoperoxidase staining. Sections of the retina, the optic nerve, and the brain were processed by the immunoperoxidase method as previously described (Sheng et al., 2004). Free-floating sections were bleached for 1 hour with 50% methanol and 1.5% hydrogen peroxide diluted with Milli-Q water at 4°C, and they were washed three times each for 15 minutes in PBS containing 0.3% Triton X-100 (PBST). The sections were preincubated for 2 hours with 10% normal goat serum (NGS) in 0.1 M PB containing 0.3% Triton X-100 (10% NGS blocking solution) at 4°C. The sections were incubated for 3 days with the anti-Wfs1 antibody diluted 1:10,000 in a 10% NGS blocking solution at 4°C. After the primary immunoreaction, primary antibody was washed out with PBST. Then the sections were incubated for 3 hours at 4°C with biotinylated antirabbit goat IgG (Dako Cytomation, Glostrup, Denmark; 1:500) in PBS containing 5% NGS. After the secondary immunoreaction the sections were washed three times each for 10 minutes in PBS and incubated for 3 hours at 4°C with a mixture of rabbit peroxidase anti-peroxidase (PAP; Dako Cytomation, 1:500) and peroxidase-conjugated streptavidin (Dako Cytomation, 1:500) in PBS containing 1% NGS (enhanced HRP-labeling reaction). Then they were washed three times each for 15 minutes in 0.05 M Tris-HCl buffer (pH 7.6) and subjected to a dark-violet-black coloring reaction with 0.02% 3,3′-diaminobenzidine tetrahydrochloride (DAB; Wako Pure Chemical Industries, Osaka, Japan) and 0.6% nickel ammonium sulfate hexahydrate in 0.05 M Tris-HCl buffer (pH 7.6) containing 0.0006% hydrogen peroxide for 10–15 minutes at 4°C. After three washes in PBS the sections were mounted onto glass slides in a 0.6% gelatin solution. After being air-dried they were dehydrated with a graded series of ethanol solutions, immersed in xylene, and embedded in NEW M · X mountant (Matsunami, Osaka, Japan).

To determine the specificity of the anti-Wfs1 antibody in sections the GST-Wfs1N chimeric protein (5 μg/mL) was incubated with the anti-Wfs1 antibody (1:10,000) for 6 hours at 4°C before incubation with sections of the retina, the optic nerve, and of the brain, and then immunohistochemistry was performed as described above. To verify the nonspecific immunoreaction by the secondary antibody (biotinylated antirabbit goat IgG), normal rabbit immunoglobulin (Dako Cytomation) was used instead of the primary antibody (anti-Wfs1). For the cytoarchitectonic analysis, adjacent series of the brain sections were subjected to Nissl staining by using cresyl violet (acetate) (Merck, Darmstadt, Germany).

Single and double immunofluorescent staining. To identify cell types expressing Wfs1, we performed double immunohistochemistry in retinal and optic nerve tissue. The monoclonal and goat polyclonal antibodies listed in Table 1 were used for additional primary antibodies. In experiments using the mouse monoclonal antibodies, free-floating sections were preincubated for 2 hours in a 10% NGS blocking solution at 4°C, then immunoreacted for 4 days with a mixture of the anti-Wfs1 antibody (1:5,000) and each of the monoclonal antibodies in a 10% NGS blocking solution at 4°C. After three rinses for 10 minutes in PBST the sections were incubated with a mixture of two secondary antibodies in PBS containing 5% NGS and 0.3% Triton X-100 for 24 hours at 4°C. The two secondary antibodies used were Alexa Fluor 488 conjugated with the $F(ab')_2$ fragment of goat antirabbit IgG (H+L) (1:200; Molecular Probes) and Alexa Fluor 594 conjugated to the $F(ab')_2$ fragment of goat antimouse IgG (H+L) (1:200; Molecular Probes). The sections were washed three times for 10 minutes in PBS and mounted onto glass slides in a 0.6% gelatin solution. After being air-dried the sections were subjected to nuclear staining by using a bisBenzimide (Hoechst 33258, Sigma-Aldrich, 0.1 mg/mL) solution, and coverslipped with Vectashield mounting medium (Vector Laboratories). For staining using the rat monoclonal antibody, Alexa Fluor 488 conjugated to goat antirabbit IgG (H+L), highly cross-absorbed (1:200; Molecular Probes) and Alexa Fluor 568 conjugated to goat antirat IgG (H+L) (1:200; Molecular Probes) were used as second-

ary antibodies. For staining using the goat polyclonal antibody, normal donkey serum was used instead of NGS. As for secondary antibodies, Alexa Fluor 488 conjugated to donkey antirabbit IgG (H+L) (1:200; Molecular Probes) and Alexa Fluor 594 conjugated to donkey antigoat IgG (H+L) (1:200; Molecular Probes) were used.

In double immunohistochemistry for detecting GFAP and GS simultaneously in the optic nerve, the rabbit polyclonal anti-GFAP antibody (1:1,000) and the mouse monoclonal anti-GS antibody (1:500) were used as primary antibody. Other procedures were the same as those for double immunohistochemistry by using the anti-Wfs1 and each of the mouse monoclonal antibodies. To eliminate the possibility of any crossreaction between secondary antibodies and primary antibodies from the wrong species, one of the two primary antibodies was removed. In these control experiments no crossreactivity was observed (data not shown).

Single immunofluorescent staining was applied to Wfs1/tracer double labeling. The anti-Wfs1 antibody (1:5,000) alone was used for primary antibody, and Alexa Fluor 488 conjugated with the $F(ab')_2$ fragment of goat antirabbit IgG (H+L) (1:200; Molecular Probes) alone for secondary antibody. Other procedures were the same as those for double immunohistochemistry by using the anti-Wfs1 and each of the mouse monoclonal antibodies. In Fluorescent Latex Microspheres injection cases a coverslip was made by using Fluoromount-G (SouthernBiothech, Birmingham, AL) instead of the Vectashield mounting medium (Vector Laboratories) in order to prevent Fluorescent Latex Microspheres from fading (manufacturer's technical information by Lumafluor).

To determine Wfs1-specific immunoreactivity in Wfs1/Goα and Wfs1/FLM double-labeling studies, the anti-Wfs1 antibody (1:5,000) was preabsorbed with the antigen (50 μg/mL) as described in the "Single immunoperoxidase staining" section.

Photomicrographs and terminology

Brightfield photomicrographs were taken using a DS-5Mc color digital camera (Nikon, Tokyo, Japan) equipped with an Eclipse 80i photomicroscope (Nikon). Fluorescence photomicrographs were taken with a FV500 confocal laser scanning microscope (Olympus, Tokyo, Japan) at the Center for Chronic Viral Diseases, Kagoshima University Graduate School of Medical and Dental Sciences, or a LSM510 (Carl Zeiss, Jena, Germany) at the Institute for Biomedical Research and Education in Yamaguchi University Science Research Center. Images were transferred to Adobe Photoshop 6 (Adobe Systems, San Jose, CA) and brightness, contrast, and picture sharpness were adjusted. No other adjustment was made.

The nomenclature used for the different regions of the brain follows that of Paxinos and Franklin (2001).

RESULTS

Immunoblot analysis of Wfs1 protein expression

To determine organ-specific Wfs1 protein expression in the brain, retina, and optic nerve, and to characterize the specificity of the anti-Wfs1 antibody, we performed immunoblot analysis. The anti-Wfs1 antibody detected Wfs1 protein bands of ≈100 kDa in extracts from the brain, retina, and optic nerve. In addition, a Wfs1-immunoreactive band of ≈70 kDa in extracts from the retina was observed (Fig. 1, anti-Wfs1). These protein bands were not seen when extracts from the brain, retina, and optic nerve were incubated with the anti-Wfs1 antibody preabsorbed by incubation with the GST-Wfs1N chimeric protein (antigen) (Fig. 1, Absorbed).

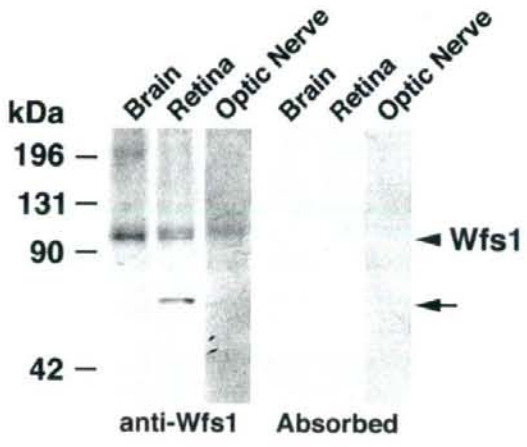

Fig. 1. Wfs1 protein immunoreactivity in the normal mouse brain, retina, and optic nerve. Immunoblot of extracts from the normal mouse brain, retina, and optic nerve probed with rabbit antimouse Wfs1 N-terminus antibody (anti-Wfs1), and with the antibody preabsorbed by incubation with GST-Wfs1 N-terminus chimeric protein (Absorbed). The arrowhead indicates Wfs1 protein bands of ≈100 kDa in extracts from the brain, retina, and optic nerve (anti-Wfs1). The arrow shows a Wfs1 immunoreactive band of ≈70 kDa in extracts from the retina (anti-Wfs1). These bands are not seen in the antibody-absorption experiment (Absorbed). Positions of size markers are indicated on the left.

Wfs1 mRNA expression in the normal mouse retina

To determine cell-specific *Wfs1* expression in retinal cells we performed RNA in situ hybridization on normal mouse retinal sections by using a mouse *Wfs1* antisense-riboprobe. The most intense *Wfs1* mRNA signals were observed in cell bodies of the ganglion cell layer (GCL; Fig. 2A). Moderate signals were distributed in the inner and outer rows of the inner nuclear layer (INL), and in the inner segment of photoreceptors (PR). The moderate signals in the outer row showed a dash-shaped appearance and were located along the boundary between the INL and outer plexiform layer (OPL). Weak signals were seen in the intermediate row of the INL and outer nuclear layer (ONL; Fig. 2A). Few detectable signals were found in control experiments with a mouse *Wfs1* cRNA sense probe. In these experiments there was a tendency for reaction deposits to be randomly scattered over the entire retina, including the inner plexiform layer (IPL; Fig. 2B).

Wfs1 protein expression in the normal mouse retina

To examine cell-specific protein localization, retinal sections were immunostained by using the anti-Wfs1 anti-

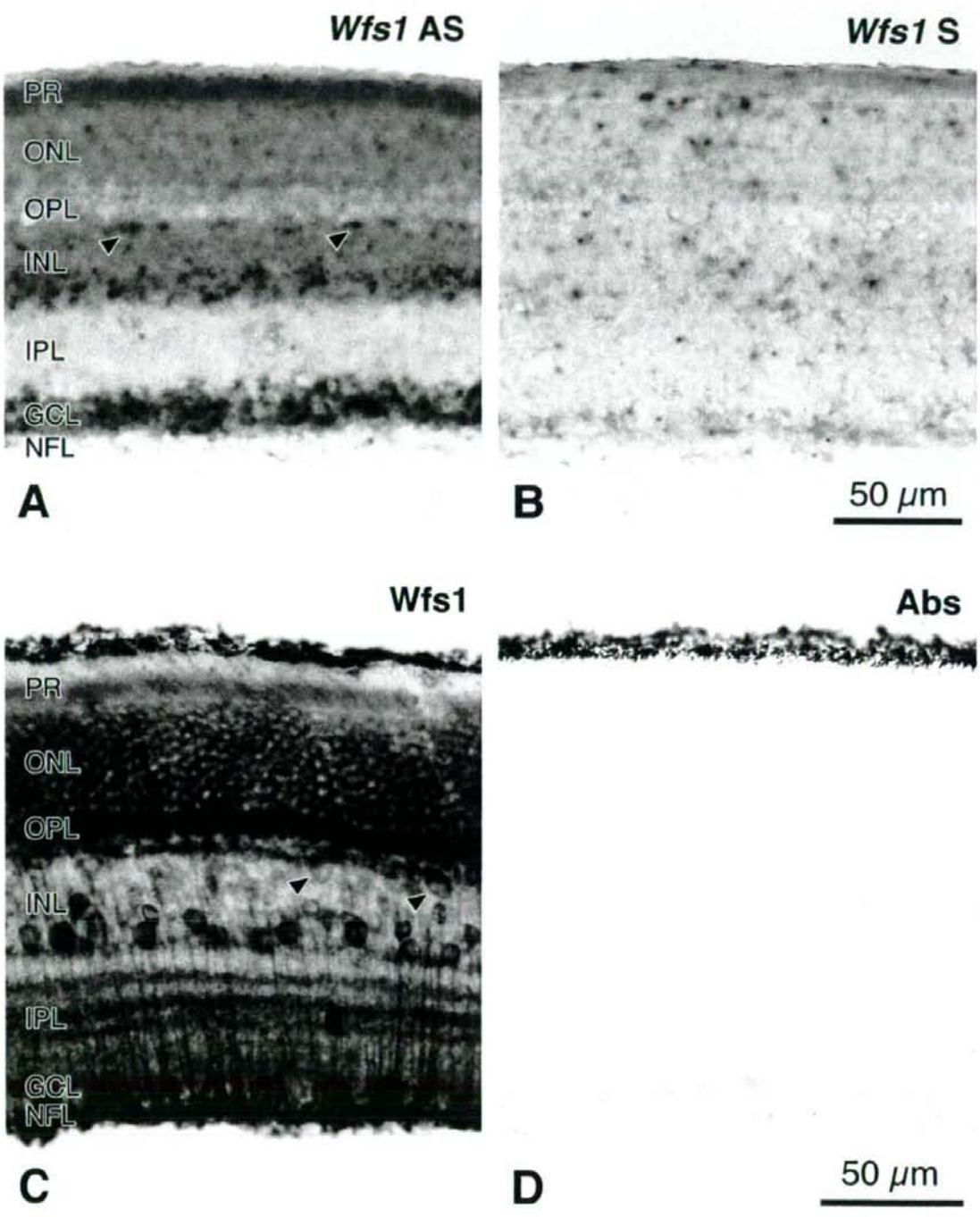

Fig. 2. *Wfs1* mRNA signals and protein immunoreactivity in the normal mouse retina. **A,B:** Mouse *Wfs1* mRNA signals in two adjacent sections of the retina hybridized with antisense cRNA probes of the mouse *Wfs1* 5'-terminus (*Wfs1* AS; A), and with sense cRNA probes (*Wfs1* S; B). Arrowheads indicate moderate *Wfs1* mRNA signals in the outer row of the inner nuclear layer (INL). **C,D:** Mouse Wfs1 protein immunoreactivity in two sections of the retina immunostained with rabbit antimouse Wfs1 N-terminus antibody (Wfs1; C), and with the antibody preabsorbed by incubation with GST-Wfs1 N-terminus chimeric protein (antigen) (Abs; D). Arrowheads indicate Wfs1-immunoreactive neurons, of which cell bodies are weakly labeled and processes are moderately labeled, in the outer row of the INL. Note that a substantial number of *Wfs1* mRNA signals and a considerable amount of protein immunoreactivity are seen not only in the ganglion cell layer but also in the inner and the outer nuclear layers of the normal mouse retina. PR, photoreceptor; ONL, outer nuclear layer; OPL, outer plexiform layer; INL, inner nuclear layer; IPL, inner plexiform layer; GCL, ganglion cell layer; NFL, optic nerve fiber layer. Scale bars = 50 μm in B,D apply to A,C, respectively.

body. The most intense immunoreactivity was observed in the OPL, the inner row of the INL, the GCL, and in the optic nerve fiber layer (NFL). Moderate immunoreactivity was found in the inner segment of PR, the ONL, and in the outer row of the INL. In the outer row of the INL, Wfs1-immunoreactive cell bodies were seen with their processes extending along the intense immunoreactivity in the OPL (arrowheads in Fig. 2C). Weakly Wfs1-immunoreactive cell bodies were seen in the middle row of the INL. In the IPL three labeled strata were observed and the immunoreactivity in the intermediate stratum was stronger than that in the other two strata. Radially extending Wfs1-immunoreactive fibers were clearly seen from the INL to the NFL with these fibers terminating at the inner limiting membrane (Fig. 2C). When a normal rabbit immunoglobulin was used instead of the anti-Wfs1 antibody, as a control for Wfs1 immunohistochemistry, no clear immunoreactivity by the secondary antibody was seen in cytoplasms of the normal mouse retina (data not shown). When the antibody preabsorbed by incubation with the GST-Wfs1N chimeric protein (antigen), no clearly immunoreactive cytoplasm was observed (Fig. 2D).

To confirm which cell types express Wfs1, retinal sections or whole-mount retinae were double-immunostained with the anti-Wfs1 antibody and with each of the antibodies against several retinal marker proteins. In the outer row of the INL, Wfs1 immunoreactivity was observed in horizontal cells, which were immunolabeled with antibodies against calbindin-D-28K (a horizontal cell marker). In these cells the intensity of Wfs1 immunoreactivity was weak-to-moderate and the immunoreactivity was seen in both cell bodies and processes (Fig. 3A–C). In the outer and intermediate rows of the INL, faint Wfs1 immunoreactivity was detected in putative ON-cone, and rod bipolar cells, which were immunolabeled with antibodies against G-protein Goα (a bipolar cell marker; Fig. 3D–F). In control (preabsorption) experiments, Wfs1 immunoreactivity was hardly seen in Goα-immunoreactive bipolar cells (Fig. 3G–I; compare 3D with 3G). In the inner row of the INL, strong Wfs1 immunoreactivity was observed in nondisplaced amacrine cells, which were immunolabeled with antibodies against ChAT (a cholinergic amacrine cell marker; Fig. 3J–L) or against calbindin-D-28K (an amacrine cell marker; Fig. 3M–O). In the IPL the three Wfs1-immunoreactive strata were overlapped with three calbindin-D-28K-immunoreactive strata (Fig. 3M–O). Out of these strata the outer and inner ones were overlaid with two cholinergic strata (Fig. 3J–L).

In the GCL, strong Wfs1 immunoreactivity was observed in cholinergic displaced amacrine cells, which were immunolabeled with antibodies against ChAT (a cholinergic amacrine cell marker; Fig. 4A–F). In addition, Wfs1-immunoreactive but noncholinergic cells were distributed in this layer (Fig. 4A–C). To examine whether these cells are RGCs, we performed Wfs1/tracer double labeling and Wfs1/retinal ganglion cell-specific-marker double immunofluorescent staining. Wfs1 immunoreactivity was detected in RGCs that were retrogradely labeled in vivo with Fluorescent Latex Microspheres (Fig. 4G–I) or with Fluoro-Ruby (Fig. 5A–C). Additionally, Wfs1 immunoreactivity was also detected in RGCs that were immunolabeled with antibodies against tubulin, βIII isoform (Fig. 4M–O), or Brn-3a POU-domain transcription factor (Fig. 4P–R). To verify whether Wfs1 immunoreactivity is positive in RGCs, we performed control (preabsorption) experiments. In these experiments, Wfs1 immunoreactivity was hardly seen in Fluorescent Latex Microspheres-labeled RGCs (Fig. 4J–L; compare 4G with 4J). There is a tendency that Wfs1 immunoreactivity in cholinergic displaced amacrine cells is stronger than that in RGCs. Thus, immunoreactivity for Wfs1 was observed in all neuron types: photoreceptors, horizontal cells, bipolar cells, nondisplaced and displaced amacrine cells, and RGCs (Figs. 3, 4, 5A–C).

In glial cells, immunoreactivity for Wfs1 was observed solely in Müller cells, which were exclusively immunolabeled with antibodies against GS. In Müller cells, Wfs1 immunoreactivity was strong in the endfeet adjacent to the inner limiting membrane, moderate in internal radial processes, but weak in their cell bodies localized to the intermediate row of the INL (Fig. 5D–F). Wfs1 immunoreactivity was not seen in GFAP-immunoreactive astrocytes, or mouse CD11b-immunoreactive microglia (Table 2).

Optic nerve

Because a definition of the optic nerve subdivision is necessary for the description and interpretation of the experimental results, we will briefly describe our criteria for determining the border of each part of the optic nerve.

Fig. 3. Cellular localization of Wfs1 in the inner nuclear layer of the normal mouse retina. **A–C:** Wfs1 immunoreactivity in horizontal cells. A retinal section was double-immunostained for Wfs1 (Wfs1; A; Alexa Fluor 488 label; green) and for a horizontal cell marker (calbindin-D-28K, CalD28K; B; Alexa Fluor 594 label; red). Cell nuclei are labeled in blue with bisBenzimide (Hoechst 33258; B,C). C is an overlaid image. Arrows indicate a horizontal cell immunoreactive for Wfs1. **D–F:** Wfs1 immunoreactivity in bipolar cells. A retinal section was double-immunostained for Wfs1 (Wfs1; D; Alexa Fluor 488 label; green) and for a bipolar cell marker (G-protein Goα, Goα; E; Alexa Fluor 594 label; red). Cell nuclei are labeled in blue with bisBenzimide (Hoechst 33258; E,F). F is an overlaid image. Arrows and arrowheads show a putative ON-cone bipolar and a rod bipolar cells that are immunoreactive for Wfs1, respectively. **G–I:** A control experiment of Wfs1 immunoreactivity in bipolar cells. An adjacent retinal section of D–F was double-immunostained for Wfs1 after a preabsorption procedure (Wfs1 Abs; G; Alexa Fluor 488 label; green) and for Goα (H; Alexa Fluor 594 label; red). Cell nuclei are labeled in blue with bisBenzimide (Hoechst 33258; H,I). I is an overlaid image. Arrows and arrowheads show a putative ON-cone bipolar and a rod bipolar cell that are not immunoreactive for Wfs1, respectively. **J–O:** Wfs1 immunoreactivity in nondisplaced amacrine cells. A retinal section was double-immunostained for Wfs1 (Wfs1; J; Alexa Fluor 488 label; green) and for a nondisplaced amacrine cell marker (choline acetyltransferase, ChAT; K; Alexa Fluor 594 label; red). Another section was double-immunostained for Wfs1 (Wfs1; M; Alexa Fluor 488 label; green) and for another nondisplaced amacrine cell marker (calbindin-D-28K, CalD28K; N; Alexa Fluor 594 label; red). Cell nuclei are labeled in blue with bisBenzimide (Hoechst 33258; N,O). L and O are overlaid images. Arrowheads indicate nondisplaced amacrine cells immunoreactive for Wfs1. These fluorescence photomicrographs were taken with an FV500 confocal microscope (Olympus). Note that Wfs1 immunoreactivity is observed in photoreceptors, horizontal cells, bipolar cells, and in nondisplaced amacrine cells. ONL, outer nuclear layer; OPL, outer plexiform layer; INL, inner nuclear layer; IPL, inner plexiform layer; GCL, ganglion cell layer. Scale bar = 20 μm in O applies to A–N.

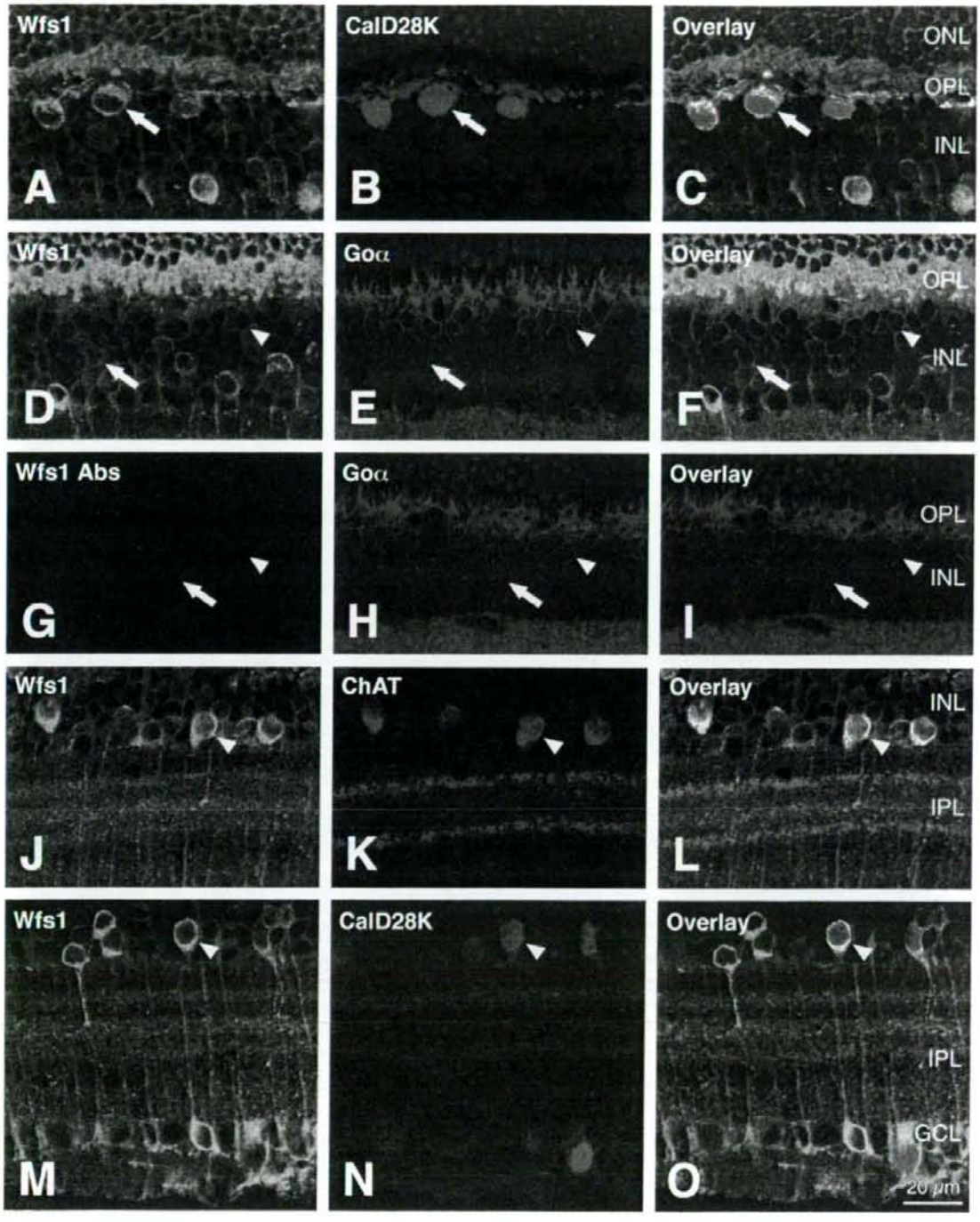
Wfs1
CalD28K
Overlay
ONL
OPL
INL
A
B
C
Wfs1
Goα
Overlay
OPL
INL
D
E
F
Wfs1 Abs
Goα
Overlay
OPL
INL
G
H
I
Wfs1
ChAT
Overlay
INL
IPL
J
K
L
Wfs1
CalD28K
Overlay
IPL
GCL
20 μm
M
N
O

Figure 3

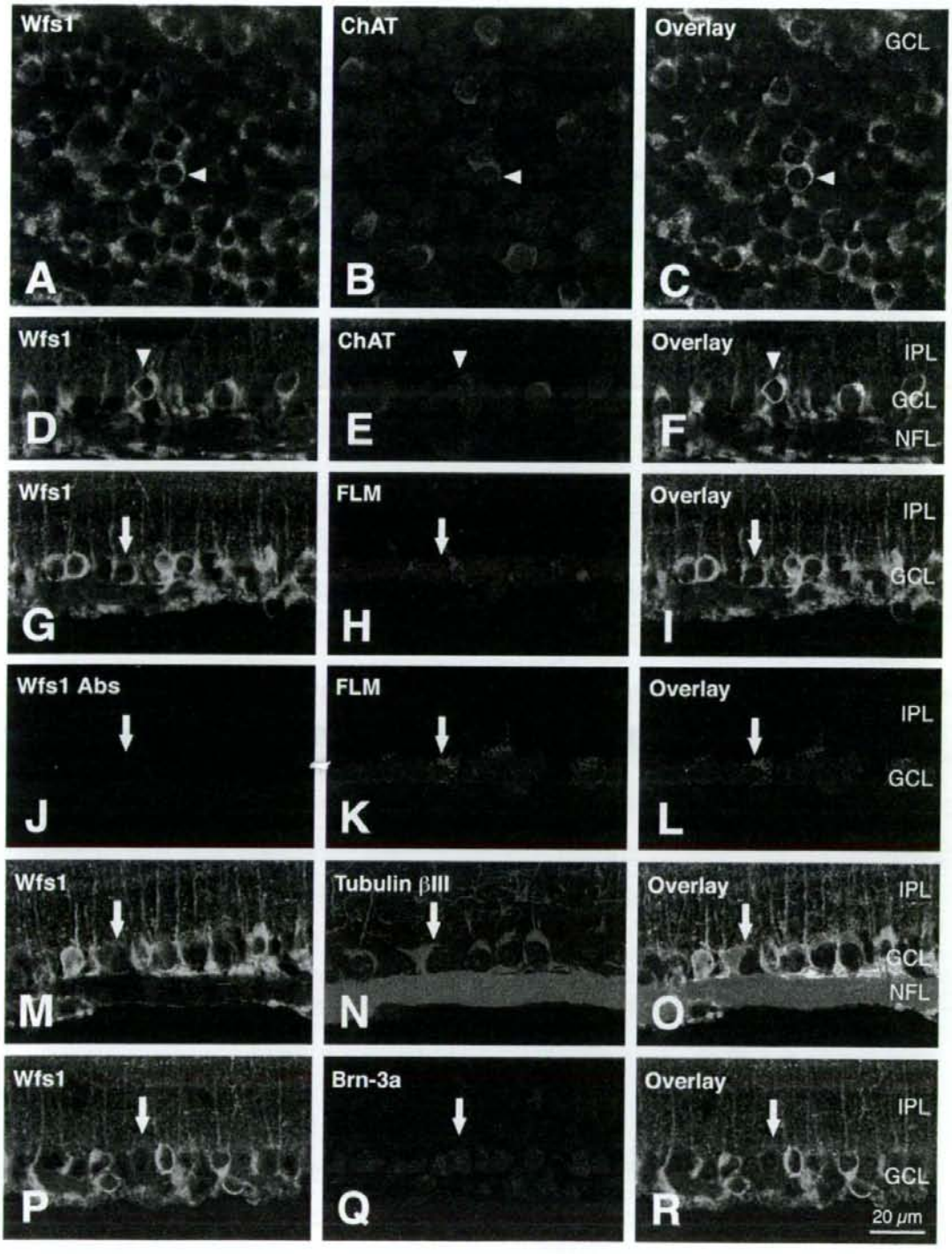
Wfs1
ChAT
Overlay
GCL
A
B
C
Wfs1
ChAT
Overlay
IPL
GCL
NFL
D
E
F
Wfs1
FLM
Overlay
IPL
GCL
G
H
I
Wfs1 Abs
FLM
Overlay
IPL
GCL
J
K
L
Wfs1
Tubulin βIII
Overlay
IPL
GCL
NFL
M
N
O
Wfs1
Brn-3a
Overlay
IPL
GCL
20 μm
P
Q
R

Figure 4

In the orbit the mouse optic nerve was divided into three parts: intraretinal (i), astrocytic filament dense (afd), and astrocytic filament sparse (afs). This classification was defined by the position of the sensory retina and by the distribution of astrocytic filaments. The border between the i and afd parts was set at the boundary between the sensory retina and the retinal pigment epithelium. Astrocytic filaments were seen to be elongated transversely at the border (Fig. 6A,C), while those in the i part were observed to be extended longitudinally. In the afd part a very high concentration of astrocytic filaments was seen. A majority of astrocytic filaments in the afs part were long and extended perpendicular to the optic nerve axis, while a minority were seen to be short and expanded parallel to the axis. The border between the afd and afs parts was defined by the distal (anterior) limit of longer transverse filaments in the afs part (Fig. 6A,C). The length of the afd part was around 200 μm. The area containing GS-immunoreactive cells in the mouse optic nerve corresponded to the afs part (Fig. 6).

Wfs1 mRNA expression in the normal mouse optic nerve

Next, to determine whether *Wfs1* mRNA is expressed in the optic nerve we performed RNA in situ hybridization on longitudinal sections of the normal mouse optic nerve by using a mouse *Wfs1* antisense-riboprobe. Weak-to-moderate *Wfs1* mRNA signals were observed in the afd and afs parts. In the afd part, *Wfs1* mRNA-hybridized cells were densely concentrated, while in the afs part they were sparsely distributed. Weak *Wfs1* mRNA signals were detected in the i part (Fig. 7A). In control experiments by using a mouse *Wfs1* cRNA sense probe few mRNA signals were observed (Fig. 7B).

TABLE 2. Distribution of Wfs1 Immunoreactivity in the Normal Mouse Retina

Retinal Cells	
Photoreceptor	–
Outer plexiform layer	–
Horizontal cells	–
Bipolar cells	–
Amacrine cells	–
Inner plexiform layer	–
Ganglion cells	+
Displaced amacrine cells	+
Muller cells	–
Astrocytes	–
Microglia	–

+, present; –, not present.

Wfs1 protein expression in the normal mouse optic nerve

We next examined cell-specific Wfs1 protein localization in the optic nerve. Weak-to-moderate Wfs1 immunoreactivity was clearly seen in the afd and afs parts (Fig. 7C,E,F). Wfs1-immunoreactive cells were aligned along optic nerve fiber bundles, and more tightly distributed in the afd than afs part. Background Wfs1 immunoreactivity on optic nerve fiber bundles was greater in the afd than afs part (Fig. 7C,E,F). Weak Wfs1 immunoreactivity was detected in the i part (Fig. 7C). When a normal rabbit immunoglobulin was used instead of the anti-Wfs1 antibody, no immunoreactivity was seen in the optic nerve (data not shown). When the antibody preabsorbed by incubation with the GST-Wfs1N chimeric protein (antigen), immunoreactivity was not observed (Fig. 7D).

To confirm which glial cell types express Wfs1, other longitudinal sections were double-immunostained with the anti-Wfs1 antibody, and with antibodies against GFAP (an astrocyte marker), oligodendrocytes [RIP] (an oligodendrocyte marker), GS (a glial cell marker), or mouse CD11b (a marker for microglia). Wfs1 immunoreactivity was observed solely in astrocytes (Fig. 8A–I). No Wfs1 immunoreactivity was found in oligodendrocytes (Fig. 8J–O), GS-immunoreactive glial cells (Fig. 8P–R), or in microglia (data not shown; Table 3).

Wfs1 mRNA expression in the normal mouse vision-related brain structures

We examined whether *Wfs1* mRNA was expressed in the optic chiasm, the optic tract, the retino-recipient nuclei, and in the visual cortex (vision-related brain structures). Moderate *Wfs1* mRNA signals were observed in layer II of the primary and secondary visual cortical areas. In layer II, moderate signals were distributed along the boundary between layers I and II, and weak signals were seen deeper down (Fig. 9A,C). In the retino-recipient nuclei, *Wfs1* mRNA signals were weak in the suprachiasmatic nucleus (SCN) and in the SC. In the SC, *Wfs1* mRNA-hybridized cells were dispersed in the zonal, superficial gray, and intermediate gray layers (Fig. 9D,F). Extremely weak or no *Wfs1* mRNA signals were seen in the optic chiasm, the optic tract, the LGN, the pretectum, and in the medial terminal nucleus (data not shown). In control experiments by using a mouse *Wfs1* cRNA sense probe, few mRNA signals were observed (data not shown).

Fig. 4. Cellular localization of Wfs1 in the ganglion cell layer of the normal mouse retina. **A–F:** Wfs1 immunoreactivity in displaced amacrine cells. A whole-mount retina (A–C) and a vertical retinal section (D–F) were double-immunostained for Wfs1 (Wfs1; A,D; Alexa Fluor 488 label; green) and for a displaced amacrine cell marker (choline acetyltransferase, ChAT; B,E; Alexa Fluor 594 label; red). Cell nuclei are labeled in blue with bisBenzimide (Hoechst 33258; B,C,E,F). C and F are overlaid images. Arrowheads indicate displaced amacrine cells immunoreactive for Wfs1. **G–I:** Wfs1 immunoreactivity in retinal ganglion cells (RGCs). Panels show a retinal section in which Wfs1 (G; Alexa Fluor 488 label; green) and Fluorescent Latex Microspheres (FLM; H; rhodamine label; red) double labeling was made. Cell nuclei are labeled in blue with bisBenzimide (Hoechst 33258; H,I). I is an overlaid image. Arrows indicate a retinal ganglion cell immunoreactive for Wfs1. **J–L:** A control experiment of Wfs1 immunoreactivity in RGCs. Wfs1 Abs; (J; Alexa Fluor 488 label; green) and FLM (K; rhodamine label; red) double labeling was performed in an adjacent retinal section of G–I after a preabsorption of the anti-Wfs1 antibody with the antigen. Cell nuclei are labeled in blue with bisBenzimide (Hoechst 33258; K,L). L is an overlaid image. Arrows indicate a retinal ganglion cell not immunoreactive for Wfs1. **M–R:** Wfs1 immunoreactivity in RGCs analyzed by double immunohistochemistry. A retinal section was double-immunostained for Wfs1 (Wfs1; M; Alexa Fluor 488 label; green) and for a ganglion cell marker (tubulin, βIII isoform, Tubulin βIII; N; Alexa Fluor 594 label; red). Another section was double-immunostained for Wfs1 (Wfs1; P; Alexa Fluor 488 label; green) and for another ganglion cell marker (Brn-3a POU-domain transcription factor, Brn-3a; Q; Alexa Fluor 594 label; red). Cell nuclei are labeled in blue with bisBenzimide (Hoechst 33258; N,O,Q,R). O and R are overlaid images. Arrows indicate RGCs immunoreactive for Wfs1. These fluorescence photomicrographs were taken with a FV500 confocal microscope (Olympus). Note that Wfs1 immunoreactivity is observed in both displaced amacrine cells and RGCs. IPL, inner plexiform layer; GCL, ganglion cell layer; NFL, optic nerve fiber layer. Scale bar = 20 μm in R applies to A–Q.

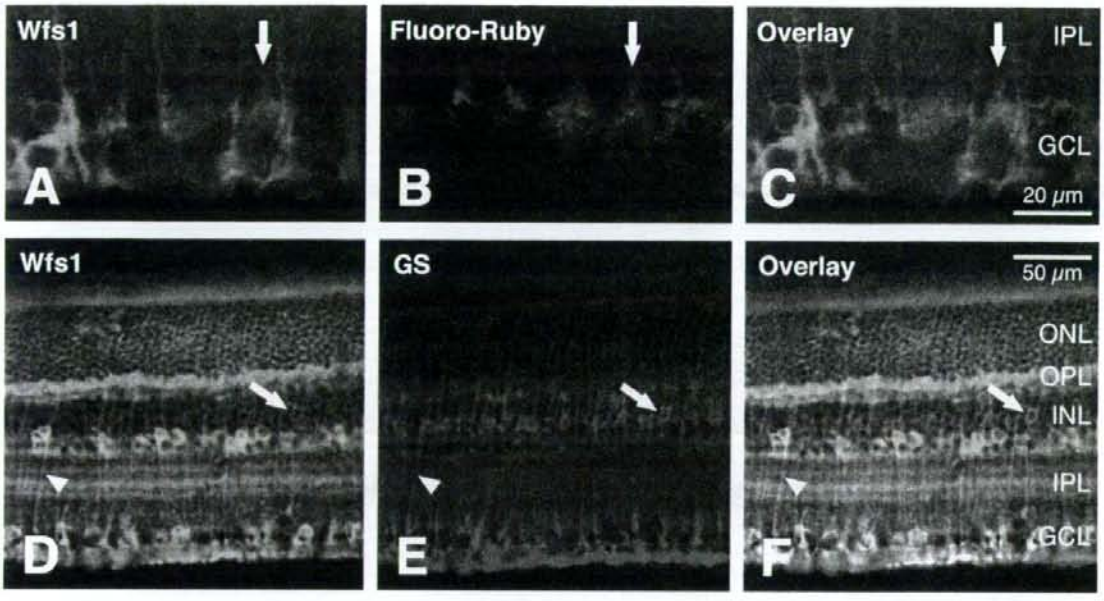

Fig. 5. Wfs1 immunoreactivity in retinal ganglion cells **(A–C)** and in Müller cells **(D–F)** of the normal mouse retina. A–C: Wfs1 (A; Alexa Fluor 488 label; green) and Fluoro-Ruby (B; tetramethylrhodamine label; red) double labeling. C is an overlaid image. Arrows indicate a retinal ganglion cell immunoreactive for Wfs1. D–F: Double immunostaining for Wfs1 (Wfs1; D; Alexa Fluor 488 label; green) and for a Müller cell marker (glutamine synthetase, GS; E; Alexa Fluor 594 label; red). F is an overlaid image. Arrows, and arrowheads show a cell body, and an inner process of Müller cells immunoreactive for Wfs1, respectively. Note that Wfs1 immunoreactivity is observed in Müller cells as well as in neurons of the retina. These fluorescence photomicrographs were taken with a LSM 510 confocal microscope (Carl Zeiss). ONL, outer nuclear layer; OPL, outer plexiform layer; INL, inner nuclear layer; IPL, inner plexiform layer; GCL, ganglion cell layer. Scale bars = 20 μm in C applies to A,B; 50 μm in F applies to D,E.

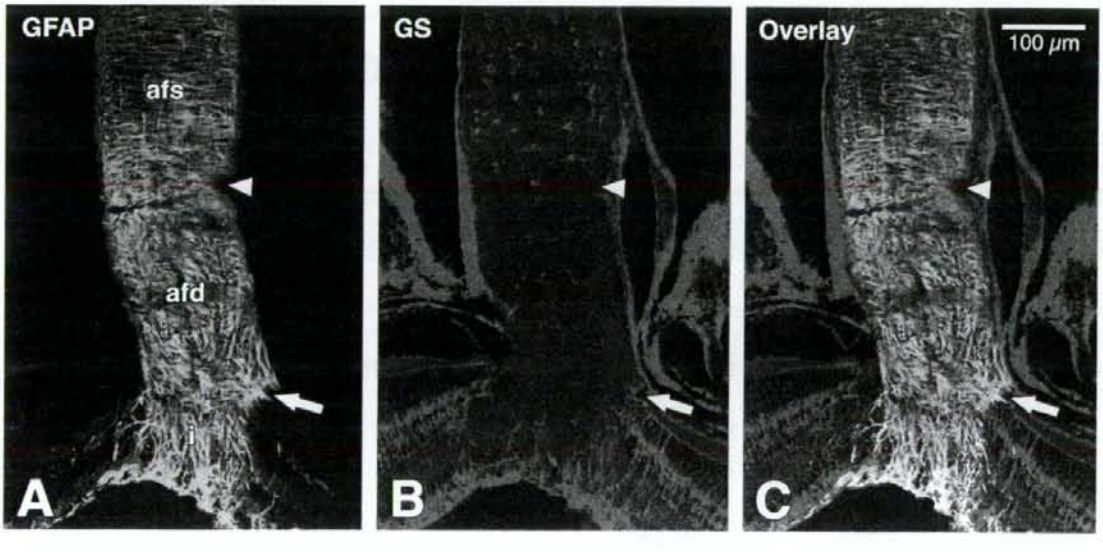

Fig. 6. Distribution of glial cells in the normal mouse optic nerve. Panels show double immunostaining for two glial cell markers, glial fibrillary acidic protein (GFAP; **A**; Alexa Fluor 488 label; green), and glutamine synthetase (GS; **B**; Alexa Fluor 594 label; red). **C**: An overlaid image. The mouse optic nerve is divided into three parts: intraretinal (i), astrocytic filament dense (afd), and astrocytic filament sparse (afs). Arrows, and arrowheads indicate the border between i and afd, and the boundary between afd and afs, respectively. These fluorescence photomicrographs were taken with a FV500 confocal microscope (Olympus). Note that the area containing GS-immunoreactive cells in the mouse optic nerve corresponds to the afs part. Scale bar = 100 μm in C applies to A,B.

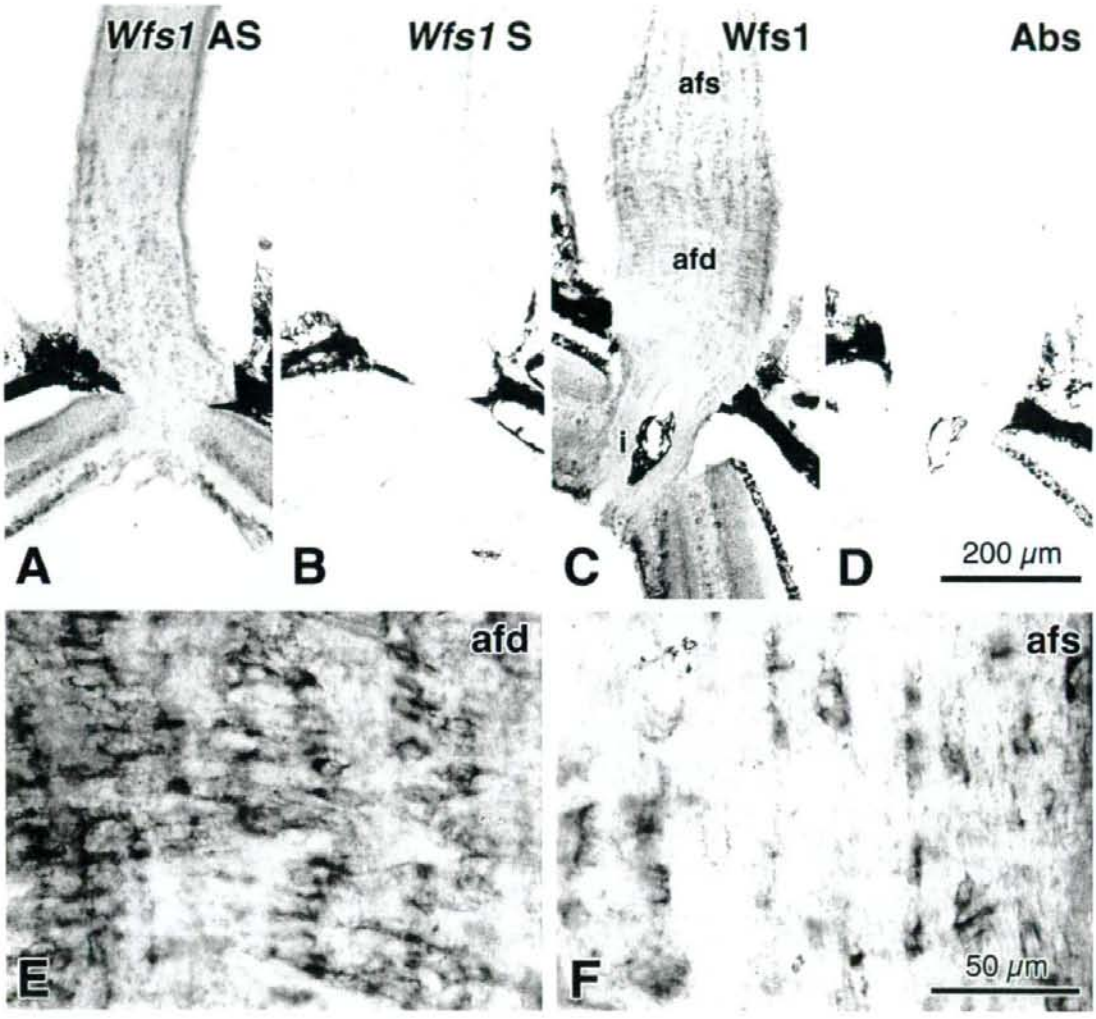

Fig. 7. *Wfs1* mRNA signals and protein immunoreactivity in the normal mouse optic nerve. **A,B:** Mouse *Wfs1* mRNA signals in two adjacent sections of the optic nerve hybridized with antisense cRNA probes of the mouse *Wfs1* 5'-terminus (*Wfs1* AS; A), and with sense cRNA probes (*Wfs1* S; B). **C,D:** Mouse Wfs1 protein immunoreactivity in two adjacent sections of the optic nerve immunostained with rabbit antimouse Wfs1 N-terminus antibody (Wfs1; C), and with the antibody preabsorbed by incubation with GST-Wfs1 N-terminus chimeric protein (antigen) (Abs; D). **E,F:** Higher magnification photomicrographs of mouse Wfs1 immunoreactivity in another adjacent section of C. E,F show Wfs1-immunoreactive cells in the astrocytic filament dense (afd) part, and those in the astrocytic filament sparse (afs) part, respectively. Note that both *Wfs1* mRNA signals and Wfs1 protein immunoreactivity are present in the mouse optic nerve. Scale bars = 200 μm in D applies to A–C; 50 μm in F applies to E.

Wfs1 protein expression in the normal mouse vision-related brain structures

We next examined whether Wfs1 protein was expressed in the vision-related brain structures. Wfs1 immunoreactivity was found in the visual cortex, the SCN, and in the SC (Figs. 9B,E, 10A). In the visual cortex, moderately Wfs1-immunoreactive neurons were distributed in layer II of the primary and secondary visual cortical areas. The more strongly immunoreactive neurons were distributed in the more superficial part of the layer. In addition, Wfs1-immunoreactive punctations were observed in layer V (Fig. 9B,C). In the SCN, moderately Wfs1-immunoreactive neurons were seen in the dorsomedial part (Fig. 10A). In the SC, moderately immunoreactive cells were distributed in the zonal, superficial gray, and intermediate gray layers (Fig.

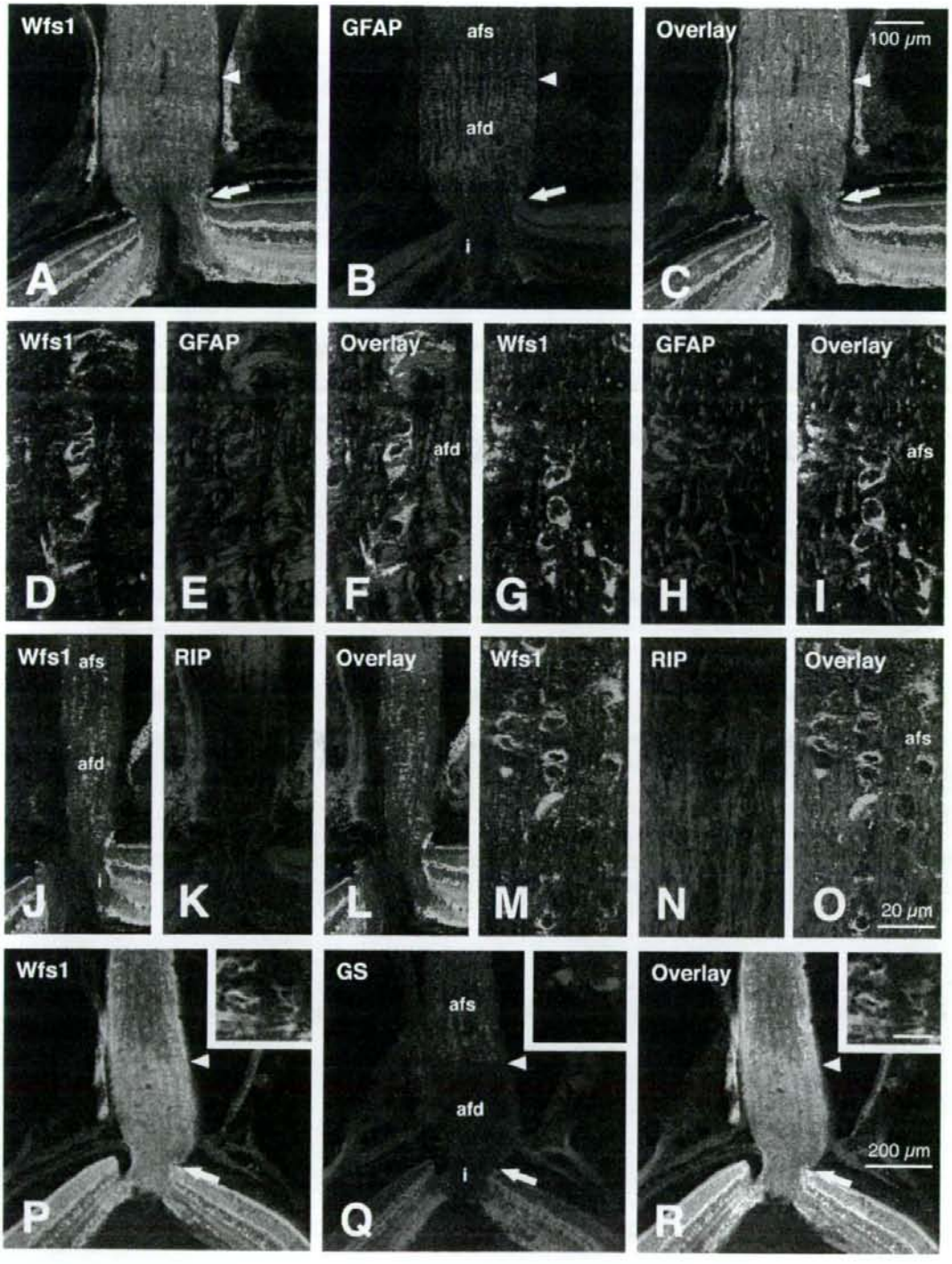
Wfs1
GFAP
afs
afd
i
Overlay
100 μm
A
B
C
Wfs1
GFAP
Overlay
afd
Wfs1
GFAP
Overlay
afs
D
E
F
G
H
I
Wfs1
afs
afd
RIP
Overlay
Wfs1
RIP
Overlay
afs
20 μm
J
K
L
M
N
O
Wfs1
GS
afs
afd
i
Overlay
200 μm
P
Q
R

Figure 8